the transgene on learning behavior, as well as to test whether the protein synthesis inhibition specifically affected long-term memory, both short-term and long-term memories were examined. At 30 min after the training, freezing response in contextual (Figure 7A) and cued conditioning (Figure 7D) was at the same level between wild-type and hip-eEF-2K-tg mice, indicating that the contextual and cued short-term memories were intact in hip-eEF-2K-tg mice. Long-term memory was examined at 1 day and 10 days after the training with two separate sets of mice. Compared to that in wild-type mice, a lower freezing rate was observed in eEF-2K-tg mice in contextual (Figure 7B and C; $p<0.001$; Student's t test), but not cued conditioning (Figure 7E and F), in both retention tests, indicating that long-term hippocampus-dependent memory, but not hippocampus-independent memory, was impaired. To exclude a possibility that a different nociceptive response might contribute to the difference above, the minimal amount of current required to produce stereotypical behaviors (flinching/running, jumping, and vocalizing) was measured after the retention tests, and the results did not show any significant difference between these mice (data not shown).

In order to determine whether the hippocampus-specific protein synthesis inhibition affected other types of hippocampus-dependent memory, spatial learning and memory were evaluated by using a Morris water-maze test [32,33]. Mice were trained with a five-day training protocol. In both wild-type and hip-eEF-2K-tg

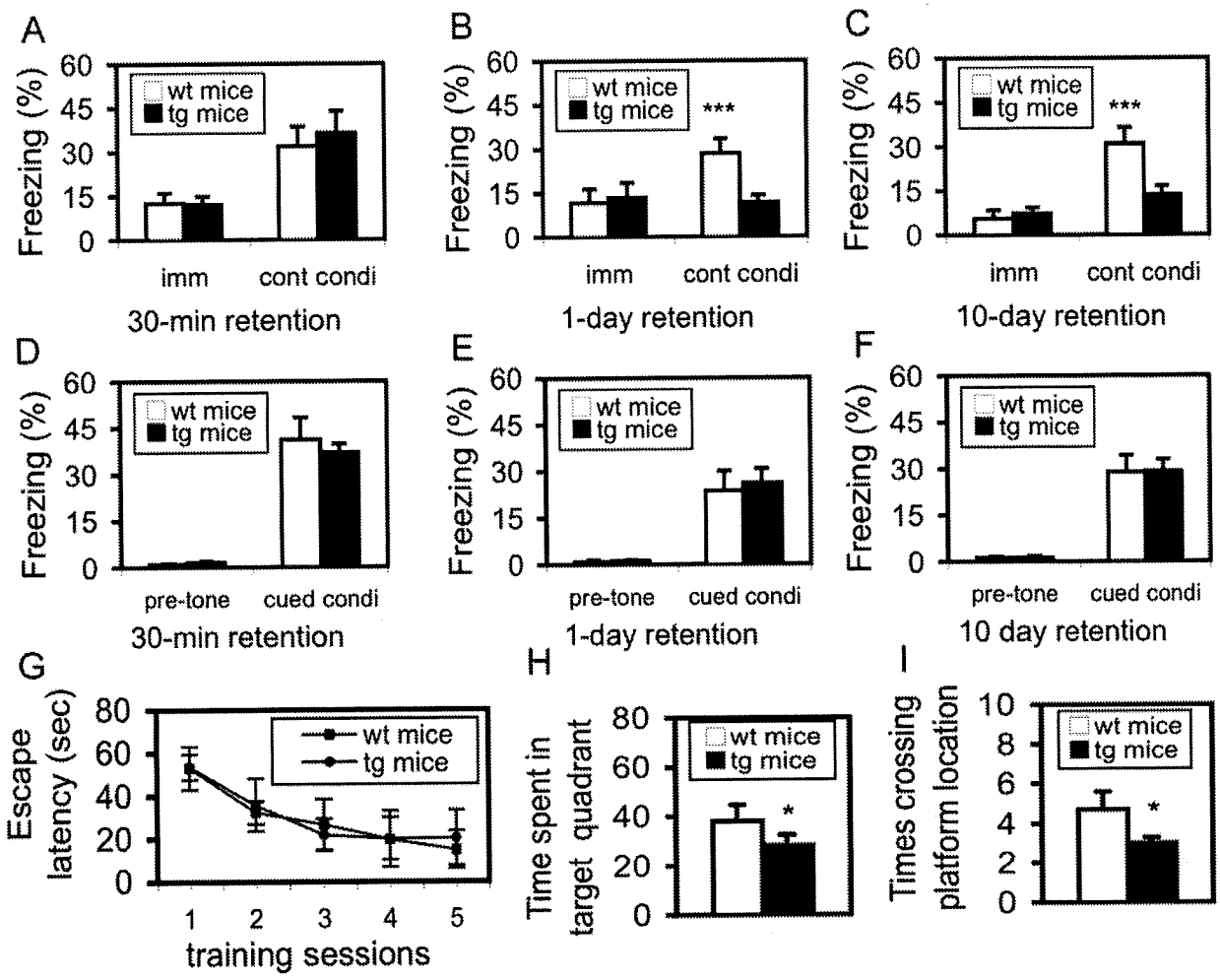

Figure 7. Long-term, but not short-term, hippocampus-dependent memory is impaired in hip-eEF-2K-tg mice. A. Short-term memory in contextual conditioning was measured at 30 min after the training. No significant difference was observed in either immediate (imm) freezing after shock or contextual conditioning (cont condi) between wild-type (wt, n = 10) and hip-eEF-2K-tg mice (tg, n = 13). **B.** Short-term memory in cued conditioning was measured at 30 min after the training. No significant difference was observed in either pre-tone freezing or cued conditioning (cued condi) between wt (n = 10) and tg mice (n = 13). **C.** Long-term memory in contextual conditioning was measured at 1 day after training. While no significant difference was observed in immediate freezing after shock, a highly significant difference was found in contextual conditioning between wt (n = 10) and tg mice (n = 12). ***, $p<0.001$, Student's t test. **D.** Long-term memory in cued conditioning was measured at 1 day after training. No significant difference was observed in either pre-tone freezing or cued conditioning. **E.** Long-term memory in contextual conditioning was measured at 10 days after the training. While no significant difference was observed in immediate freezing after shock, a highly significant difference was found in contextual conditioning between wt (n = 11) and tg mice (n = 12). ***, $p<0.001$, Student's t test. **F.** Long-term memory in cued conditioning was measured at 10 days after training. No significant difference was observed in either pre-tone freezing or cued conditioning. **G.** Learning curve in a water maze test; repeated ANOVA did not reveal a significant difference between wt (n = 11) and tg (n = 12) mice. **H.** Time spent in the target quadrant in a probe test 24 hr after the completion of the training sessions. *, $p<0.05$, Student's t test. **I.** Number of crossing over the platform location in the probe test 24 hr after the completion of the training session. *, $p<0.05$, Student's t test.
doi:10.1371/journal.pone.0007424.g007

mice, the escape latency dramatically decreased following the training (Figure 7G), and cross-sectional analyses with an one-way ANOVA revealed a highly significant difference in the latency in either wild-type [$F(4,50) = 6.74$, $p<0.001$] or hip-eEF-2K-tg mice [$F(4,55) = 7.59$, $p<0.001$]. Moreover, a repeated ANOVA did not reveal any significant difference between these two groups, indicating that all these mice could equally learn the task. In a probe test, however, a significant difference ($p<0.05$; Student's *t* test) in the amount of time spent in the target quadrant (Figure 7H) or in the number of crossing the area that represented the location of the platform previously placed during the training sessions (Figure 7I) was observed, indicating that the transgenic mice were impaired in spatial retention. Since the learning curve (training sessions) represents a compound effect of acquisition and retention, with a dominant influence from the acquisition, a normal learning curve in hip-eEF-2K-tg mice indicates an intact acquisition process. On the other hand, the probe test detects the "pure" retention of the spatial navigation, and a deficit in this test provides additional evidence that these transgenic mice are impaired in long-term hippocampus-dependent (spatial) memory.

Late-phase LTP (L-LTP) was impaired in the hippocampus of hip-eEF-2K-tg mice

LTP, a cellular model for learning and memory, may also be divided into different phases. Evidence indicates that these different phases perfectly fit into memory stages [34]. Early-phase LTP, which is protein synthesis-independent, correlates to short-term memory, whereas L-LTP, which is protein synthesis-dependent, correlates to long-term memory [35,36]. Therefore, it is important to examine whether the inhibition of protein synthesis affected L-LTP. As shown in Figure 8A, 4 trains of high-frequency stimulation (100 Hz for 1 second) were used to produce L-LTP in the hippocampal Schaffer collateral/commissural pathway. As shown in Figure 8B, it was apparently that the post-tetanic potentiation in hip-eEF-2K-tg slices was not significantly different from that in wild-type slices. This also indicated that the basal synaptic transmission was similar in all these mice. However, quantitative analyses revealed a highly significant difference between wild-type and hip-eEF-2K-tg slices from 90 min up to the whole observation period (180 min), whereas no significant difference was observed in LTP production (peak) or LTP maintenance before 90 min. These results indicated that L-LTP was specifically and significantly impaired in hip-eEF-2K-tg mice.

Discussion

In this study, we first found that dephospho-eEF-2 in both the hippocampus and amygdala of mice was temporarily associated with post-training, whereas no any significant change in the expression of the mRNAs for translational machineries or their related molecules could be identified. The use of MK-801 then revealed that both post-training dephospho-eEF-2 and memory consolidation were neuronal activity-dependent, and that there was a functional link between these two events. At the last, by using a unique transgenic mouse model, we have documented that the post-training dephospho-eEF-2 is a molecular underpinning for protein synthesis pertinent to memory consolidation.

New protein synthesis is required for various forms of long-lasting synaptic plasticity. Although the exact mechanisms might be different in different forms of plasticity, protein synthesis itself is basically under the control of both the transcriptional and translational actions. At the transcriptional level, the expression of mRNAs may directly affect protein synthesis at a number of ways. For example, a changed expression level of the translational machineries or their related molecules such as a up-regulation of mTOR [37] or a down-regulation of eEF-2K [38] may facilitate the overall translational activity. However, our genome-wide screening study did not reveal any evidence to support that this is the case for memory consolidation. Another way is that the expression of certain mRNAs may directly lead to new protein synthesis. We indeed found that the expression of certain genes such as c-fos and BDNF was up regulated following the behavioral training, which is consistent with many other studies [39,40]. Because the expression of c-fos and BDNF is critically involved in memory formation [41,42], and because most of these up-regulated transcripts may be further processed for protein synthesis, the expression of these genes may certainly contribute to memory consolidation. However, evidence indicates that the expression of these non-translational machinery-related molecules is unable to fully explain how protein synthesis is regulated for memory consolidation [43,44].

The finding that the training facilitates dephospho-eEF-2 sheds light on a new translational mechanism, which has been validated from several angles in this study. First, the dephospho-eEF-2 is coincided in the hippocampus and amygdala, both brain regions are importantly involved in consolidating fear memories [24]. Second, the post-training antagonism of NMDA receptors is able to concurrently block the dephosphorylation and memory consolidation, indicating a functional link between them. Third, as the NMDA receptor is the most important excitatory machinery in the brain, this concurrent effect indicates that both the post-training dephospho-eEF-2 and memory consolidation are neuronal activity-dependent, which is also supported by other reports [25,45–47]. Fourth, blockade of the dephospho-eEF-2 by the eEF-2K transgene dramatically inhibits protein synthesis, and this effect is more robust during an ongoing protein synthesis process that is associated with neuronal activity (Figure 5). Given that both neuronal activity and protein synthesis are critically involved in memory consolidation [15,24,25], a stronger effect during an ongoing protein synthesis process than during the general conditions provides a basis to identify whether a dynamic process of protein synthesis is more importantly required for memory consolidation. Indeed, we found that while these transgenic mice looked undistinguishable from their wild-type littermates at the overall level (Figure S2), both L-LTP and long-term hippocampus-dependent memory were significantly impaired (Figure 7 and Figure 8). All these results indicate that the post-training dephospho-eEF-2 plays a critical role in triggering memory consolidation-associated protein synthesis.

It should be mentioned that previous studies have found that the phospho-eEF-2 occurs within 15 min following the activation of NMDA receptors, and this phosphorylation is accompanied by protein synthesis inhibition [45,48]. In contrast, we found here that the antagonism of NMDA receptor led to phospho-eEF-2 at 2 hr after the treatment. Therefore, we suggest that there might be two distinct phases, an early phase of phospho-eEF-2 and a late phase of dephospho-eEF-2, following the activation of NMDA receptors. Indeed, a late phase of dephospho-eEF-2, together with an enhanced overall protein synthesis, was found in those previous studies too [45,48]. This "two-phase theory" may explain why the phospho-eEF-2 and inhibition of protein synthesis were observed within 1 hr after LTP production in the hippocampus [49], while in our study, it is supposingly that the L-LTP (after 3 hr) should be featured by an increase in dephospho-eEF-2. Another issue is about the effect of phospho-eEF-2. Although the overall protein synthesis is inhibited after the phospho-eEF-2, the expression of several specific molecules including Ca^{2+}-calmodulin-dependent

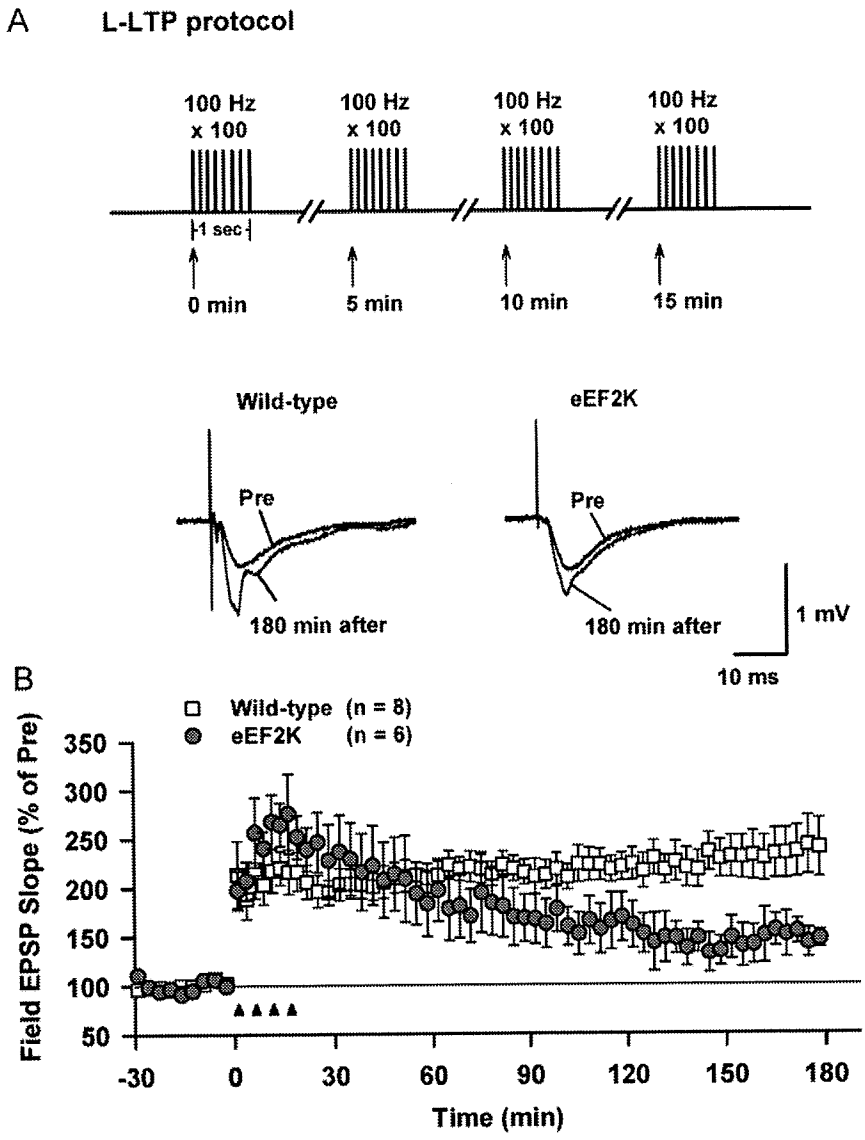

Figure 8. L-LTP, but not post-tetanic potentiation, is impaired in the hippocampus of hip-eEF-2K-tg mice. A. Four trains of high-frequency stimulation (100 Hz for 1 second) made the fEPSP still robust measured at 180 min after the stimulation in wild-type (wt) slices but not in transgenic (tg) slices. **B.** Quantitative analysis of the potentiation during this 180 min period indicated that there was no significant difference in LTP production (peak) and LTP maintenance before 90 min, whereas there was a highly significant difference exhibited from 90 min up to the whole observation period.
doi:10.1371/journal.pone.0007424.g008

kinase II (CaMK-II) [45], Arc, and c-Fos [49] is up-regulated, which is inconsistent to our results (Figure 5). Given that (1) the increase of CaMK-II is found at the synaptic level [48]; (2) the expression of Arc and c-Fos may facilitate transcriptions of other genes; and (3) the increase of the translation of Arc and c-Fos occurs at the early phase of the phospho-eEF-2, a "synaptic competition" theory[48] might explain for this discrepancy, that is the up-regulation of Arc and c-Fos in their studies may represent a competitive mechanism for a late phase enhancement of protein synthesis. In our transgenic mice, as the transgene is constitutively expressed and as the phospho-eEF-2 is persistently higher, this compensative mechanism no longer exists, and thus the translation of Arc and c-Fos is inhibited. Regarding why a protein synthesis inhibitor could block early-phase LTP [50,51], while the deficit in our transgenic mice was only observed at the L-LTP, it might be due to a different neuronal activity between these different conditions. The use of a protein synthesis inhibitor is generally accompanied by a higher synaptic function [52], while in our transgenic mice, the synaptic function may be persistently lower due to the constitutive transgene expression and thus, we could not identify a significant effect on the early-phase LTP.

Another important insight from the current study is that our study has demonstrated the requirement of new protein synthesis for memory consolidation from different angles. As described above, the role of protein synthesis in memory consolidation was originally established based on pharmacological studies with protein synthesis inhibitors [14,15,53]. Because the inhibitors are able to break the "chain" of the protein synthesis reaction, protein synthesis cannot be completed, which, in turn, renders the process of consolidation impaired. Virtually, all of those studies were essentially looking at the "consequences after the chain is broken", but could not look into "how the chain works under the normal

condition". Recently, studies focusing on translational mechanisms have revealed some new insights. For example, either pharmacologically [54,55] or genetically [56] blocking mTOR in the animals impairs memory consolidation. However, those studies are essentially similar to the pharmacological studies described above since those studies could not identify an active process that triggers protein synthesis for memory consolidation. In contrast, dephospho-eEF-2 following the behavioral training represents an active molecular process in the brain, and blocking this process leads to impairments in both L-LTP and long-term memory formation.

Why eEF-2 is dephosphorylated following the behavioral training is still unclear. Based on the findings that dephospho-eEF-2 is neuronal activity-dependent [45–47,57], together with our findings that antagonism of NMDA receptors prevents both dephospho-eEF-2 and memory consolidation, we have reasons to speculate that this dephosphorylation is learning-triggered neuronal activity-dependent. Previous studies did find that phosphorylation of mTOR and p70S6 kinase was increased following training, but they could not demonstrate whether the phosphorylation itself was essential, since they did not have an approach to specifically block the phosphorylation in the brain [58]. Based on the role of both eIF and eEF in protein synthesis, the dephospho-eEF-2 might not be the only mechanism. Recent evidence indeed indicated that phosphorylation/dephosphorylation of eIF was importantly involved in memory consolidation, while the results were inconsistent. Reduced phosphorylation of eIF2a by point mutation or by knocking out GCN2 (an eIF2a inhibitor) enhanced and impaired long-term memory, respectively [46,59,60], indicating that either the role of eIF is still unclear or that there may be a bi-directional role for phosphorylation of eIF in regulating protein synthesis [59]. In contrast, our studies have consistently shown the role of post-training dephospho-eEF-2 in memory consolidation from the behavioral, pharmacological, and genetic levels. Importantly, as eEF-2K-mediated phospho-eEF-2 is a major mechanism for the control of the rate of protein synthesis [23], post-training dephospho-eEF-2 may represent a fundamental mechanistic process that leads other translation mechanisms to promote protein synthesis for consolidation of newly learned information.

We need to point out that the effects of the transgene in the current study do not actually indicate the role of a single gene in memory consolidation, and do not essentially explore the role of a genetic basis for learning and memory in this study, as many other studies did [61], [62]. The high expression level of the transgene should not be a "physiological condition" in anyway. However, this high expression level could be used as a tool to prevent training-induced dephospho-eEF-2 in a specific brain region–the hippocampus. The results of this blockage suggested that there might be a mechanism that works at the network level to control the process of learning and memory, especially memory consolidation [63]. The answer to this question will be the next topic of our study.

Materials and Methods

All the experiments for the use of mice were performed according to the protocols approved by the Animal Care and Use Committee in Louisiana State University Health Science Center at New Orleans, and conformed with National Institutes of Health guidelines.

Fear-conditioning training

The procedures for training in FCT were the same as described previously [33]. Briefly, the conditioned stimulus (CS) was a tone at 90 dB and 2,800 Hz, and the unconditioned stimulus (US) was foot shock at 0.8 mA. During training, adult mice [2–3 months old; either B6/CBA F1 mice (from the Jackson Laboratory) or hip-eEF-2K-tg mice and their wild-type littermates] were individually put into the shock chamber and were allowed to freely explore the environment for 150 sec in the chamber. Afterward, the CS was delivered for 30 sec, and at the last 2 sec of the CS, the US was delivered. After the CS/US pairing, mice were allowed to staying in the chamber for another 30 sec and then were returned to their homecages.

cDNA microarray

The procedures for cDNA microarrays were the same as described previously [64]. Briefly, three groups of adult (2–3 months old) B6/CBA F1 mice, together with a group of naïve control mice (the same strain; without shock, but with exposure to the shock chamber), were sacrificed at 30, 60, and 120 min after the training in the FCT, respectively. The total RNA was extracted from the hippocampi and amygdalae with Trizol (Invitrogen) and was purified with RNEasy columns (Qiagen). Reverse transcription (RT) was performed using the SuperScript® III First-Strand synthesis system (Invitrogen). All samples were hybridized in duplicate to Affymetrix 420 2.0 Array Chips, which was conducted by the Core Facility at the University of Chicago. The same cDNA microarray was repeated in three individual mice. The array expression values were generated using Affymetrix Microarray Suite 5.0 and dChip analyzer 1.3.

Quantitative analysis of dephospho-eEF-2

Protein lysates were prepared from the hippocampi, amygdalae, and cortices of three groups of mice that were respectively sacrificed at 30 min, 2 hr, and 4 hr after the training in FCT. To exclude any non-specific effects, four control conditions were designed: naïve control (NC; mice were sacrificed without any treatment), shock control (SC; mice were sacrificed immediately after receiving the US), contextual control (CC; mice were sacrificed 30 min, 2 hr, or 4 hr after being exposed to the shock chamber for 5 min but without shock), and tone control (TC; mice were sacrificed 30 min, 2 hr, or 4 hr after being exposed to the CS). A total of 100 μg of protein lysates from each sample was separated by an SDS-PAGE (8%) and then was transferred onto Immobilon-P membranes (Millipore). The membranes were incubated with either anti-phospho-eEF-2 antibody (1:2,000) or anti-total eEF-2 antibody (1:2,000; all from Cell Signaling and Technology Laboratories), followed by HRP-conjugated secondary antibody (1:4,000; Jackson ImmunoReseach). Blotting signal was visualized with the ECL detection system (Pierce). The same membranes were re-probed to anti-β-actin antibody (1:10000, Santa Cruz Biotechnology Inc). Densitometry was performed using Image J Analysis software (version 1.39c). The phosphorylation ratio (%) was calculated as: (total eEF-2 - phospho-eEF-2)/total eEF-2 X 100. In order to minimize the artificial signal, the exposure time was the same for the membranes used to detect the total eEF-2 and phospho-eEF-2. The dephospho-eEF-2 ratio (%) after the training was calculated as: [phospho-eEF-2 of naive hippocampus (or amygdala) - phospho-eEF-2 of trained hippocampus (or amygdala)/phospho-eEF-2 of naive (or amygdala) X 100%]. The change in the total eEF-2 ratio was calculated as: [total eEF-2 of wild-type hippocampus (or amygdala) - total eEF-2 of transgenic hippocampus (or amygdala)/total eEF-2 of wild-type hippocampus (or amygdala) X 100%]. The expression level in each sample was normalized to the expression level of β-actin before the calculation. The quantitative data were the average of the levels from 5–6 mice, with at least 2 measures in each animal.

NMDA receptor antagonism

An NMDA receptor antagonist, MK-801 (St. Louis, MO; 0.2 mg/kg), was administered (i.p.) immediately after the training in FCT. Both contextual and cued conditionings were examined at 2 hr or 24 hr after the MK-801 treatment with two separate sets of mice. The procedures for memory retention test are described below. Another three groups of mice (naïve/vehicle, training/MK-801, and training/vehicle) were used for immunoblotting experiments, in order to determine the phospho-eEF-2 level as described above.

Generation of hip-eEF-2K-tg mice

An advanced transgenic approach was used in this study. Two independent transgenic mouse strains were needed. One was Cre transgenic mouse strain, in which the expression of the Cre recombinase was under the control of ∂-CaMK-II promoter. An 8.5 kb of ∂-CaMK-II promoter was used to drive a 2.6 kb of *Not I* transgene cassette that consisted of a 0.6 kb exon-intron splicing signal, a 0.4 kb element encoding a nuclear localization signal (pBS317), a 1.029 kb Cre cDNA, and a 0.6 kb poly-A signals (pNN265). All these components were subcloned into a pBS(−) vector. Due to some locus effects, the random insertion of ∂-CaMK-II promoter into the mouse genome could generate different expression patterns of the transgene. In our Cre transgenic mice, the expression of Cre was exclusively observed in most parts of the hippocampus. The other mouse strain was eEF-2K transgenic mice, in which the expression of the eEF-2K transgene was under the control of a chicken β-actin promoter so that the transgene would express in all types of cells. However, a transcriptional silencer (stop sequence) was put upstream of the eEF-2K cDNA to silence its transcription. Moreover, this stop sequence was flanked by two loxP elements. A recombination by the Cre recombinase led to the deletion of the stop sequence so that the expression of the eEF-2K transgene occurred in the brain regions where Cre expressed. The eEF-2K cDNA was cloned from the total RNA extracted from a brain of a B6/CBA F1 mouse with the primers of 5′-GCA ACA TGG CAG ACG AAG ACC TCA TC-3′ and 5′ GGG GCA GTT ATT CCT CCA TCT GGG CC-3′. The cDNA was confirmed by sequencing. The eEF-2K cDNA was flanked by an artificial intron and SV-40 poly-A signal, all from pNN265, in order to ensure a correct translation and to make the transgene distinguishable from the endogenous eEF-2K gene. Embryo donors and foster mothers were all from B6/CBA F1 mice (Jackson Laboratory), in order to (1) have a similar genomic background between transgenic mice and their wild-type littermates, (2) have a better genetic background for behavioral analysis, and (3) have a comparable genetic background to the non-transgenic studies as shown in Figure 2. After being linearized with appropriate restriction enzymes, the expression cassette was injected into the pro-nuclei of B6/CBA F1 zygotes to produce transgenic founders. The transgene copy number in the founders was determined by Southern blots (data not shown). In order to have a higher expression level of the eEF-2K transgene, a founder with a gene copy number of about 12 of the eEF-2K transgene was bred into Cre transgenic mice to produce double transgenic mice. The genotypes of mice were determined by PCR analyses of the genomic DNA from the tails, which respectively detected the Cre transgene and the eEF-2K transgene.

in situ hybridization. The procedures for *in situ* hybridization were the same as described previously [33]. Briefly, an oligo probe (5′- CAC CAC AGA AGT AAG GTT CCT TCA CAA AGA TCC TCT AGC-3′) that specifically recognized the eEF-2K transgene only was 35S-labeled. Coronal brain sections (20 μm) were made with a Cryostat (Leica, CM 1900), and the hybridization was the same as described in our previous publication [33]. After being washed, the brain sections were exposed to Kodak Hyperfilm^{TM} MP film. The hybridization signal was visualized with an Olympus B X 51 TF microscope and analyzed with the Q-imaging system.

Histology

The procedures for histological experiments were the same as described previously [65]. Briefly, mice were anesthetized with sodium pentobarbital (Sigma-Aldrich) and were perfused transcardially with 0.9% saline followed by 4% paraformaldehyde (PFA). Brains were removed and post-fixed overnight with 4% PFA in 30% sucrose. Coronal brain sections (40 μm) were made with the Cryostat and were then used for Nissl (cresyl violet) staining. For Golgi-impregnated staining, mice were anesthetized and perfused transcardially with 0.9% saline followed by 4% PFA. Brains were kept in Golgi-Cox solution with light-tighten for 6 days and then in 30% sucrose for another 2–3 days. Brains were mounted on sectioning stages with cyanocacrylic glue. A vibratome (Leica, VT1200) was used to make brain sections (200 μm), which were then mounted onto 2% gelatinized microscope slides. Once mounted, the blotted slides were kept in a humidity chamber until ready to be stained. For staining, the slides were placed in glass staining tray and processed as following: (1) Rinsed in distilled water for 1 min; (2) Placed in ammonium hydroxide for 30 min in the dark; (3) Rinsed in distilled water for 1 min; (4) Placed in Kodak Fix for film for 30 min in the dark; (5) Rinsed in distilled water for 1 min; and (6) Dehydration with 50% to 100% EtOH for a couple of times at each steps, and then were mounted with a cover-lip.

Protein synthesis under the normal conditions

L-[35S]-methionine incorporation rate was examined, in order to evaluate protein synthesis. Both hip-eEF-2K-tg and wild-type littermate mice were treated (i.p.) with a single dose of L-[35S]-methionine (150 μCi/animal, specific activity 151 Ci/mmol, GE Healthcare), and were sacrificed 2 hr after the treatment by decapitation. For quantitative analysis, brain tissues including the hippocampus and cortex (control) were quickly dissected from brains and protein lysates were prepared for liquid scintillation analysis as described elsewhere [29]. The concentration of L-[35S]- methionine incorporation into proteins in these tissues was calculated based on tissue weight. To map the brain region-specific protein synthesis, serial coronal brain sections (20 μm) were made on the Cryostat and autoradiography of L-[35S]-methionine incorporation (exposed to Kodak Hyperfilm^{TM} MP film, Amersham for 10 days) was conducted as described elsewhere [66]. The -[35S]- methionine incorporation signal was analyzed with an Olympus microscope (SZ-PT) and the Q-imaging system.

Protein synthesis under the conditions of enhanced neuronal activity

To evoke neuronal activity in the hippocampus, both hip-eEF-2K-tg and wild-type mice were treated (i.p.) with a single dose of KA (Sigma; 20 mg/kg), a non-NMDA receptor agonist, and were divided into 5 sub-groups. Behavioral responses were observed in their homecages and these five groups of mice were then sacrificed at a time-course of 5, 30, 60 120, and 180 min after the KA-treatment. The total RNA and protein lysates were extracted from the whole hippocampi of mice. Real-time RT-PCR (Applied Biosystem, 7900th) was used to determine the mRNA expression level for Arc and c-fos. Two customized fluorescence-labeled

probes that recognized Arc and c-fos, respectively, were used. After RT, each reaction contained 5 μl Taqman Universal PCR Mastermix in a total volume of 10 μl containing 1.25 μl RT production. PCR reactions were conducted under the condition of 95°C for 10 min followed by 40 cycles of 30 sec at 95°C and 1 min at 60°C. The expression levels for both Arc and c-fos were normalized with 18S rRNA level. Final quantitative analysis was based on two measures (duplicate samples) in each mouse with a total of at least 4 mice in each group. Western blots were used to determine the expression of Arc and c-Fos at the protein level as described above. The concentrations of the anti-Arc antibody and anti-c-Fos antibody were both at 1:2000 and these antibodies were purchased from Cell Signaling Technology Inc. The amount of protein loading was normalized by β-actin immunoblotting. Quantitative analysis was based on two measures in each mouse and in each group at least 5 mice were examined. The comparison of the ratio between the mRNA expression and protein expression within the same animal as well as the comparison of the difference in this ratio between wild-type and hip-eEF-2K-tg mice would provide a valuable means to test the specific inhibition at the translational level.

Short-term and long-term memory

Both FCT and water maze test were used to examine memory functions [33]. For the FCT, both wild-type and hip-eEF-2K-tg mice (2–3 months old, with both female and male mice mixed) were trained with a one-trial protocol. For short-term memory, a retention test was conducted 30 min after the training. Both contextual and cued conditionings were examined. For contextual conditioning, mice were individually put back into the chamber where they received CS/US pairing, and freezing responses were recorded for 5 min with a sampling method at an interval of 5 sec. For cued conditioning, mice were individually put into a novel chamber and 3 min later, the same tone that was used during the training session was delivered for 3 min. Freezing responses were recorded in both pre-tone and during-tone periods. Freezing was defined as no movement of any part of the body, except for respiration. For long-term memory, every test was the same as described above, except for that the intervals between the training and retention test were 1 day and 10 days, respectively, with the use of two separate sets of animals. For the Morris water-maze test, a water tank with 1 meter in diameter and a computerized video-tracking system were used. A training protocol of 5 training sessions was used. Each training session per day contained 4 trials, with each trial lasting for 60 sec. The order of the quadrants for each mouse being released into the water tank was randomly designed for each session. The interval between each two trials was about 1 hr. After each trial, mice were towel dried and were immediately returned to their homecages. Escape latency to the platform, swimming speed, and swimming path were automatically recorded and the data were analyzed by a Nodel navigation tracking system (EthoVision, Pro-Noldus). One probe test was conducted 24 hr after the completion of all training sessions. During the probe test, the platform was removed, and mice were individually allowed to swimming in the pool for 60 sec. Time spent in each quadrant and times crossing over the place that the platform was previously located during the training sessions were recorded to determine long-term spatial memory.

Open-field behaviors in hip-eEF-2K-tg mice

Open-field behaviors were examined by using an automatic-recording open-field working station (MED Associates, Georgia, VT) as described in our previous publication [67]. Briefly, the open-field box was illuminated by a dim light (20 lux) and two sets of 16 pulse-modulated infrared photobeams were placed on opposite walls 2.5 cm apart to record X-Y ambulatory movements. Mouse behaviors in the box were computer-interfaced at a sampling rate of 100-ms resolution. Before testing, mice were transported into the behavioral room to adapt to the environment for at least 1 hr. Behavioral responses of mice in the box were recorded for 60 min. The total path length and rearing times were recorded automatically.

Electrophysiology

The procedures for electrophysiological recording were described in our previous publication [68]. Briefly, transverse hippocampal slices (400 μm) were cut from brains of wild-type and hip-eEF-2K-tg mice (2–3 months old), kept submerged at 27°C–28°C, and superfused (1–2 ml/min) with oxygenated (95% O2, 5% CO2) artificial cerebrospinal fluid (ACSF). Bipolar tungsten stimulating electrodes were placed in the CA1&3 to stimulate the Schaffer collateral and commissural fibers, and extracellular field EPSPs (fEPSPs) were recorded with a glass microelectrode (2–3 MU, filled with 2 M NaCl) positioned in the hippocampus. Baseline stimulation frequency was 2 min-1, and the intensity of the 0.1 ms pulses was adjusted to evoke 35%–40% maximal fEPSPs. Tetanic LTP was induced by high-frequency stimulation in brief trains (100 Hz, 1 s) applied either as a single train or four trains separated by 5 min intervals. To reduce day-to-day variability, simultaneous recordings were obtained from two slices. Data were recorded from wild-type and hip-eEF-2K-tg slices. The experimenters were blind to the mouse genotype.

Statistical Analyses

Dada was analyzed by Student's *t* test or one-way ANOVA followed by the Bonferroni *post hoc* test wherever it was appropriate. A p value that was less than 0.05 was considered significance.

Supporting Information

Figure S1 Constructs for transgenic mice. A. Expression vector for the Cre transgenic mice, which consists of an 8.5 kb of α-CaMKII promoter and a 2.6 kb Not I fragment encoding Cre gene. B. Expression vector for eEF-2K transgenic mice, which consists of a chicken β-actin promoter (3.1 kb), a stop signal that is flanked by two loxP elements (1.5 kb) and an eEF-2K cDNA that is flanked by an artificial intron and SV-40 poly-A signal.
Found at: doi:10.1371/journal.pone.0007424.s001 (1.44 MB TIF)

Figure S2 Open-field behaviors in hip-eEF-2K-tg mice. A. Total movement time. B. Total travel time. C. Rearing numbers. No significant difference was found in any of these indexes between wild-type (wt, n = 11) and hip-eEF-2K-tg (tg, n = 12) mice. Cent: center area; Peri: peripheral area.
Found at: doi:10.1371/journal.pone.0007424.s002 (1.74 MB TIF)

Acknowledgments

Part work was done in the University of Chicago, IL, USA.

Author Contributions

Conceived and designed the experiments: AN YPT. Performed the experiments: HII AN BG XX TM MZ YPT. Analyzed the data: HII MZ YPT. Contributed reagents/materials/analysis tools: EG. Wrote the paper: HII YPT.

References

1. Abel T, Lattal KM (2001) Molecular mechanisms of memory acquisition, consolidation and retrieval. Curr Opin Neurobiol 11: 180–187.
2. Mayes AR, Roberts N (2001) Theories of episodic memory. Philos Trans R Soc Lond B Biol Sci 356: 1395–1408.
3. McGaugh JL (2000) Memory–a century of consolidation. Science 287: 248–251.
4. Richardson JT (2007) Measures of short-term memory: a historical review. Cortex 43: 635–650.
5. Bourtchuladze R, Frenguelli B, Blendy J, Cioffi D, Schutz G, et al. (1994) Deficient long-term memory in mice with a targeted mutation of the cAMP-responsive element-binding protein. Cell 79: 59–68.
6. Germano C, Kinsella GJ (2005) Working memory and learning in early Alzheimer's disease. Neuropsychol Rev 15: 1–10.
7. Friedman D, Nessler D, Johnson R, Jr. (2007) Memory encoding and retrieval in the aging brain. Clin EEG Neurosci 38: 2–7.
8. Lombroso P, Ogren M (2009) Learning and memory, part II: molecular mechanisms of synaptic plasticity. J Am Acad Child Adolesc Psychiatry 48: 5–9.
9. Davis HP, Squire LR (1984) Protein synthesis and memory: a review. Psychol Bull 96: 518–559.
10. Gold PE (2007) Protein synthesis inhibition and memory: Formation vs amnesia. Neurobiol Learn Mem.
11. Holahan MR, Routtenberg A (2007) Post-translational synaptic protein modification as substrate for long-lasting, remote memory: an initial test. Hippocampus 17: 93–97.
12. Quevedo J, Vianna MR, Martins MR, Barichello T, Medina JH, et al. (2004) Protein synthesis, PKA, and MAP kinase are differentially involved in short- and long-term memory in rats. Behav Brain Res 154: 339–343.
13. Wanisch K, Tang J, Mederer A, Wotjak CT (2005) Trace fear conditioning depends on NMDA receptor activation and protein synthesis within the dorsal hippocampus of mice. Behav Brain Res 157: 63–69.
14. Luft AR, Buitrago MM, Ringer T, Dichgans J, Schulz JB (2004) Motor skill learning depends on protein synthesis in motor cortex after training. J Neurosci 24: 6515–6520.
15. Schafe GE, LeDoux JE (2000) Memory consolidation of auditory pavlovian fear conditioning requires protein synthesis and protein kinase A in the amygdala. J Neurosci 20: RC96.
16. Gingras AC, Raught B, Sonenberg N (1999) eIF4 initiation factors: effectors of mRNA recruitment to ribosomes and regulators of translation. Annu Rev Biochem 68: 913–963.
17. Browne GJ, Proud CG (2002) Regulation of peptide-chain elongation in mammalian cells. Eur J Biochem 269: 5360–5368.
18. Raught B, Gingras AC, Sonenberg N (2001) The target of rapamycin (TOR) proteins. Proc Natl Acad Sci U S A 98: 7037–7044.
19. Schalm SS, Fingar DC, Sabatini DM, Blenis J (2003) TOS motif-mediated raptor binding regulates 4E-BP1 multisite phosphorylation and function. Curr Biol 13: 797–806.
20. Ryazanov AG, Shestakova EA, Natapov PG (1988) Phosphorylation of elongation factor 2 by EF-2 kinase affects rate of translation. Nature 334: 170–173.
21. Dorovkov MV, Pavur KS, Petrov AN, Ryazanov AG (2002) Regulation of elongation factor-2 kinase by pH. Biochemistry 41: 13444–13450.
22. Nairn AC, Bhagat B, Palfrey HC (1985) Identification of calmodulin-dependent protein kinase III and its major Mr 100,000 substrate in mammalian tissues. Proc Natl Acad Sci U S A 82: 7939–7943.
23. Ryazanov AG (1993) Translational Regulation of Gene Expression II Plenum, New York: pp 295–318.
24. LeDoux JE (2000) Emotion circuits in the brain. Annu Rev Neurosci 23: 155–184.
25. Shimizu E, Tang YP, Rampon C, Tsien JZ (2000) NMDA receptor-dependent synaptic reinforcement as a crucial process for memory consolidation. Science 290: 1170–1174.
26. Mitsui K, Brady M, Palfrey HC, Nairn AC (1993) Purification and characterization of calmodulin-dependent protein kinase III from rabbit reticulocytes and rat pancreas. J Biol Chem 268: 13422–13433.
27. Santini E, Muller RU, Quirk GJ (2001) Consolidation of extinction learning involves transfer from NMDA-independent to NMDA-dependent memory. J Neurosci 21: 9009–9017.
28. McDonald RJ, Hong NS, Craig LA, Holahan MR, Louis M, et al. (2005) NMDA-receptor blockade by CPP impairs post-training consolidation of a rapidly acquired spatial representation in rat hippocampus. Eur J Neurosci 22: 1201–1213.
29. Millecamps S, Julien JP (2004) [35S]Methionine metabolic labeling to study axonal transport of neuronal intermediate filament proteins in vivo. Methods Cell Biol 78: 555–571.
30. Vendrell M, Curran T, Morgan JI (1998) A gene expression approach to mapping the functional maturation of the hippocampus. Brain Res Mol Brain Res 63: 25–34.
31. Plath N, Ohana O, Dammermann B, Errington ML, Schmitz D, et al. (2006) Arc/Arg3.1 is essential for the consolidation of synaptic plasticity and memories. Neuron 52: 437–444.
32. Davis S, Butcher SP, Morris RG (1992) The NMDA receptor antagonist D-2-amino-5-phosphonopentanoate (D-AP5) impairs spatial learning and LTP in vivo at intracerebral concentrations comparable to those that block LTP in vitro. J Neurosci 12: 21–34.
33. Tang YP, Shimizu E, Dube GR, Rampon C, Kerchner GA, et al. (1999) Genetic enhancement of learning and memory in mice. Nature 401: 63–69.
34. Winder DG, Mansuy IM, Osman M, Moallem TM, Kandel ER (1998) Genetic and pharmacological evidence for a novel, intermediate phase of long-term potentiation suppressed by calcineurin. Cell 92: 25–37.
35. Kelly A, Mullany PM, Lynch MA (2000) Protein synthesis in entorhinal cortex and long-term potentiation in dentate gyrus. Hippocampus 10: 431–437.
36. Frey U, Huang YY, Kandel ER (1993) Effects of cAMP simulate a late stage of LTP in hippocampal CA1 neurons. Science 260: 1661–1664.
37. Chenal J, Pierre K, Pellerin L (2008) Insulin and IGF-1 enhance the expression of the neuronal monocarboxylate transporter MCT2 by translational activation via stimulation of the phosphoinositide 3-kinase-Akt-mammalian target of rapamycin pathway. Eur J Neurosci 27: 53–65.
38. Diggle TA, Redpath NT, Heesom KJ, Denton RM (1998) Regulation of protein-synthesis elongation-factor-2 kinase by cAMP in adipocytes. Biochem J 336 (Pt 3): 525–529.
39. D'Agata V, Cavallaro S (2002) Gene expression profiles–a new dynamic and functional dimension to the exploration of learning and memory. Rev Neurosci 13: 209–219.
40. Vecsey CG, Hawk JD, Lattal KM, Stein JM, Fabian SA, et al. (2007) Histone deacetylase inhibitors enhance memory and synaptic plasticity via CREB:CBP-dependent transcriptional activation. J Neurosci 27: 6128–6140.
41. Reijmers LG, Perkins BL, Matsuo N, Mayford M (2007) Localization of a stable neural correlate of associative memory. Science 317: 1230–1233.
42. Miyashita T, Kubik S, Lewandowski G, Guzowski JF (2007) Networks of neurons, networks of genes: An integrated view of memory consolidation. Neurobiol Learn Mem.
43. Richter JD, Sonenberg N (2005) Regulation of cap-dependent translation by eIF4E inhibitory proteins. Nature 433: 477–480.
44. Allison DB, Cui X, Page GP, Sabripour M (2006) Microarray data analysis: from disarray to consolidation and consensus. Nat Rev Genet 7: 55–65.
45. Scheetz AJ, Nairn AC, Constantine-Paton M (2000) NMDA receptor-mediated control of protein synthesis at developing synapses. Nat Neurosci 3: 211–216.
46. Sutton MA, Taylor AM, Ito HT, Pham A, Schuman EM (2007) Postsynaptic decoding of neural activity: eEF2 as a biochemical sensor coupling miniature synaptic transmission to local protein synthesis. Neuron 55: 648–661.
47. Carroll M, Warren O, Fan X, Sossin WS (2004) 5-HT stimulates eEF2 dephosphorylation in a rapamycin-sensitive manner in Aplysia neurites. J Neurochem 90: 1464–1476.
48. Scheetz AJ, Nairn AC, Constantine-Paton M (1997) N-methyl-D-aspartate receptor activation and visual activity induce elongation factor-2 phosphorylation in amphibian tecta: a role for N-methyl-D-aspartate receptors in controlling protein synthesis. Proc Natl Acad Sci U S A 94: 14770–14775.
49. Chotiner JK, Khorasani H, Nairn AC, O'Dell TJ, Watson JB (2003) Adenylyl cyclase-dependent form of chemical long-term potentiation triggers translational regulation at the elongation step. Neuroscience 116: 743–752.
50. Kelleher RJ, 3rd, Govindarajan A, Jung HY, Kang H, Tonegawa S (2004) Translational control by MAPK signaling in long-term synaptic plasticity and memory. Cell 116: 467–479.
51. Banko JL, Poulin F, Hou L, DeMaria CT, Sonenberg N, et al. (2005) The translation repressor 4E-BP2 is critical for eIF4F complex formation, synaptic plasticity, and memory in the hippocampus. J Neurosci 25: 9581–9590.
52. Fonseca R, Nagerl UV, Bonhoeffer T (2006) Neuronal activity determines the protein synthesis dependence of long-term potentiation. Nat Neurosci 9: 478–480.
53. Debiec J, LeDoux JE, Nader K (2002) Cellular and systems reconsolidation in the hippocampus. Neuron 36: 527–538.
54. Blundell J, Kouser M, Powell CM (2008) Systemic inhibition of mammalian target of rapamycin inhibits fear memory reconsolidation. Neurobiol Learn Mem 90: 28–35.
55. Helmstetter FJ, Parsons RG, Gafford GM (2008) Macromolecular synthesis, distributed synaptic plasticity, and fear conditioning. Neurobiol Learn Mem 89: 324–337.
56. Hoeffer CA, Tang W, Wong H, Santillan A, Patterson RJ, et al. (2008) Removal of FKBP12 Enhances mTOR-Raptor Interactions, LTP, Memory, and Perseverative/Repetitive Behavior. Neuron 60: 832–845.
57. Steward O (1997) mRNA localization in neurons: a multipurpose mechanism? Neuron 18: 9–12.
58. Bekinschtein P, Katche C, Slipczuk LN, Igaz LM, Cammarota M, et al. (2007) mTOR signaling in the hippocampus is necessary for memory formation. Neurobiol Learn Mem 87: 303–307.
59. Costa-Mattioli M, Gobert D, Stern E, Gamache K, Colina R, et al. (2007) eIF2alpha phosphorylation bidirectionally regulates the switch from short- to long-term synaptic plasticity and memory. Cell 129: 195–206.
60. Costa-Mattioli M, Gobert D, Harding H, Herdy B, Azzi M, et al. (2005) Translational control of hippocampal synaptic plasticity and memory by the eIF2alpha kinase GCN2. Nature 436: 1166–1173.
61. Flint J (1999) The genetic basis of cognition. Brain 122 (Pt11): 2015–2032.
62. Crawley JN (2008) Behavioral phenotyping strategies for mutant mice. Neuron 57: 809–818.

63. Flint J, Mott R (2008) Applying mouse complex-trait resources to behavioural genetics. Nature 456: 724–727.
64. Lazarov O, Robinson J, Tang YP, Hairston IS, Korade-Mirnics Z, et al. (2005) Environmental enrichment reduces Abeta levels and amyloid deposition in transgenic mice. Cell 120: 701–713.
65. Chen Q, Nakajima A, Choi SH, Xiong X, Tang YP (2008) Loss of presenilin function causes Alzheimer's disease-like neurodegeneration in the mouse. J Neurosci Res 86: 1615–1625.
66. Baubet V, Grange E, Sermet E, Giaume M, Gay N, et al. (1996) Widespread increase in brain protein synthesis following acute immobilization stress in adult rat brain. Neurosci Lett 219: 187–190.
67. Chen Q, Nakajima A, Meacham C, Tang YP (2006) Elevated cholecystokininergic tone constitutes an important molecular/neuronal mechanism for the expression of anxiety in the mouse. Proc Natl Acad Sci U S A 103: 3881–3886.
68. Zhao MG, Toyoda H, Lee YS, Wu LJ, Ko SW, et al. (2005) Roles of NMDA NR2B subtype receptor in prefrontal long-term potentiation and contextual fear memory. Neuron 47: 859–872.

RAGE-mediated signaling contributes to intraneuronal transport of amyloid-β and neuronal dysfunction

Kazuhiro Takuma[a,b], Fang Fang[c], Wensheng Zhang[c,d], Shiqiang Yan[c,e], Emiko Fukuzaki[b], Heng Du[c], Alexander Sosunov[c], Guy McKhann[c], Yoko Funatsu[b], Noritaka Nakamichi[b,f], Taku Nagai[b,g], Hiroyuki Mizoguchi[b,g], Daisuke Ibi[b,g], Osamu Hori[h], Satoshi Ogawa[h], David M. Stern[i], Kiyofumi Yamada[b,g,1], and Shirley ShiDu Yan[c,1]

[a]Laboratory of Medicinal Pharmacology, Graduate School of Pharmaceutical Sciences, Osaka University, Osaka 565-0871, Japan; [b]Laboratory of Neuropsychopharmacology, Division of Life Sciences, Graduate School of Natural Science and Technology, Kanazawa University, Kanazawa 920-1192, Japan; [c]Departments of Pathology, Surgery, Neurosurgery, and Taub Institute for Research on Alzheimer's Disease and the Aging Brain, College of Physicians and Surgeons, Columbia University, New York, NY 10032; [d]Institute of Natural Medicine and Chinese Medicine Resources, Beijing Normal University, Beijing 100875, China; [e]College of Chemistry and Chemical Engineering, Lanzhou University, Lanzhou 730000, China; [f]Laboratory of Molecular Pharmacotherapeutics, Division of Life Sciences, Graduate School of Natural Science and Technology, Kanazawa University, Kanazawa 920-1192, Japan; [g]Department of Neuropsychopharmacology and Hospital Pharmacy, Nagoya University Graduate School of Medicine, Nagoya 466-8560, Japan; [h]Department of Neuroanatomy, Kanazawa University Graduate School of Medical Science, Kanazawa 920-8641, Japan; and [i]VP and Dean's Office, University of Cincinnati College of Medicine, Cincinnati OH 45267

Edited by Leslie Lars Iversen, University of Oxford, Oxford, United Kingdom, and approved September 23, 2009 (received for review May 22, 2009)

Intracellular amyloid-β peptide (Aβ) has been implicated in neuronal death associated with Alzheimer's disease. Although Aβ is predominantly secreted into the extracellular space, mechanisms of Aβ transport at the level of the neuronal cell membrane remain to be fully elucidated. We demonstrate that receptor for advanced glycation end products (RAGE) contributes to transport of Aβ from the cell surface to the intracellular space. Mouse cortical neurons exposed to extracellular human Aβ subsequently showed detectable peptide intracellularly in the cytosol and mitochondria by confocal microscope and immunogold electron microscopy. Pretreatment of cultured neurons from wild-type mice with neutralizing antibody to RAGE, and neurons from RAGE knockout mice displayed decreased uptake of Aβ and protection from Aβ-mediated mitochondrial dysfunction. Aβ activated p38 MAPK, but not SAPK/JNK, and then stimulated intracellular uptake of Aβ-RAGE complex. Similar intraneuronal co-localization of Aβ and RAGE was observed in the hippocampus of transgenic mice overexpressing mutant amyloid precursor protein. These findings indicate that RAGE contributes to mechanisms involved in the translocation of Aβ from the extracellular to the intracellular space, thereby enhancing Aβ cytotoxicity.

β-amyloid | Alzheimer's disease | mitochondrial dysfunction | p38 MAPK

Alzheimer's disease (AD) is a progressive neurodegenerative process characterized by senile plaques, neurofibrillary tangles, and neuronal loss (1, 2). Deposition of amyloid-β peptide (Aβ), a 39–43-amino acid peptide derived from the transmembrane amyloid precursor protein (APP), is found in extracellular senile plaque cores and is associated with neurodegeneration in later stages of AD. In contrast, recent studies suggest that accumulation of intraneuronal Aβ may be an early event in the pathogenesis of AD (3–16). Addition of Aβ to human neuronal-like cells caused significant mitochondrial damage (17). Furthermore, our recent study revealed that binding of Aβ to Aβ-binding alcohol dehydrogenase (ABAD) or cyclophilin D (10, 11) intracellularly triggered events leading to neuronal apoptosis through a mitochondrial pathway (12, 13, 18, 19). However, mechanisms through which Aβ produced at the plasma membrane and released into the extracellular space reaches the intracellular milieu remain to be elucidated.

Receptor for advanced glycation end products (RAGE) is a multiligand receptor of the Ig superfamily of cell surface molecules (20–22). RAGE acts as a counter-receptor for several quite distinct classes of ligands, such as AGEs, S100/calgranulins, HMG1 (high mobility group 1 or amphoterin), and the family of crossed β-sheet fibrils/macromolecular assemblies, which activate receptor-mediated signal transduction pathways. These ligand-receptor interactions are believed to exert pathogenic effects through sustained cellular perturbation in a range of chronic disorders, including the secondary complications of diabetes, inflammation, and neurodegenerative processes (23, 24). RAGE, a cell surface binding site for Aβ (25), is expressed at higher levels in an Aβ-rich environment (26, 27). Targeted neuronal overexpression of a wild-type RAGE transgene in AD-type mice also expressing mutant human APP (mAPP) amplified Aβ-mediated neuronal dysfunction. The latter was shown by early abnormalities in spatial learning/memory and exaggerated neuropathologic changes not seen in single transgenics (such as transgenics expressing mAPP alone at the same ages). These data support the hypothesis that RAGE might function as a cofactor for Aβ-induced neuronal perturbation in AD (28). Interaction of Aβ with RAGE expressed on brain endothelial cells initiates cellular signaling leading to the trafficking of monocytes across the blood-brain barrier (BBB) (29). Furthermore, RAGE has been shown to mediate Aβ transport across the BBB and to contribute to pathologic accumulation of the amyloid peptide in brain (30). Herein, we demonstrate that RAGE contributes to translocation of Aβ across the cell membrane from the extracellular to the intracellular space in cortical neurons. We also present evidence that Aβ-initiated RAGE signaling, especially stimulation of p38 mitogen-activated protein kinase (MAPK), has the capacity to drive a transport system delivering Aβ as a complex with RAGE to the intraneuronal space.

Results

Extracellular Aβ Translocates into Mitochondria in Cortical Neurons. We have recently demonstrated that Aβ, endogeneously generated from a mutant APP transgene, interacts with ABAD within mitochondria and leads to apoptosis-like cell death in vivo and in vitro using a murine system (12, 13). Addition of exogenous Aβ, both 1–40 ($Aβ_{1–40}$) and 1–42 ($Aβ_{1–42}$), to culture media caused mitochondrial dysfunction and apoptotic-like cell death in cortical neurons prepared from wild-type and transgenic (Tg) ABAD mice (Fig. S1). However, evidence of Aβ-induced neuronal perturbation was significantly enhanced in the ABAD-expressing cells, indicating that an enzyme in the mitochondrial matrix (ABAD) appears to exert toxic effects in response to the exogenous Aβ. These data

Author contributions: K.T., D.M.S., K.Y., and S.S.Y. designed research; K.T., F.F., W.Z., S.Y., E.F., H.D., A.S., G.M., Y.F., N.N., T.N., H.M., and D.I. performed research; K.T., F.F., E.F., N.N., O.H., and S.O. contributed new reagents/analytic tools; K.T., F.F., and E.F. analyzed data; and K.T. and S.S.Y. wrote the paper.

Conflict of interest statement: D. Stern is a consultant for TransTech Pharma.

This article is a PNAS Direct Submission.

[1]To whom correspondence may be addressed. E-mail: sdy1@columbia.edu or kyamada@med.nagoya-u.ac.jp.

This article contains supporting information online at www.pnas.org/cgi/content/full/0905686106/DCSupplemental.

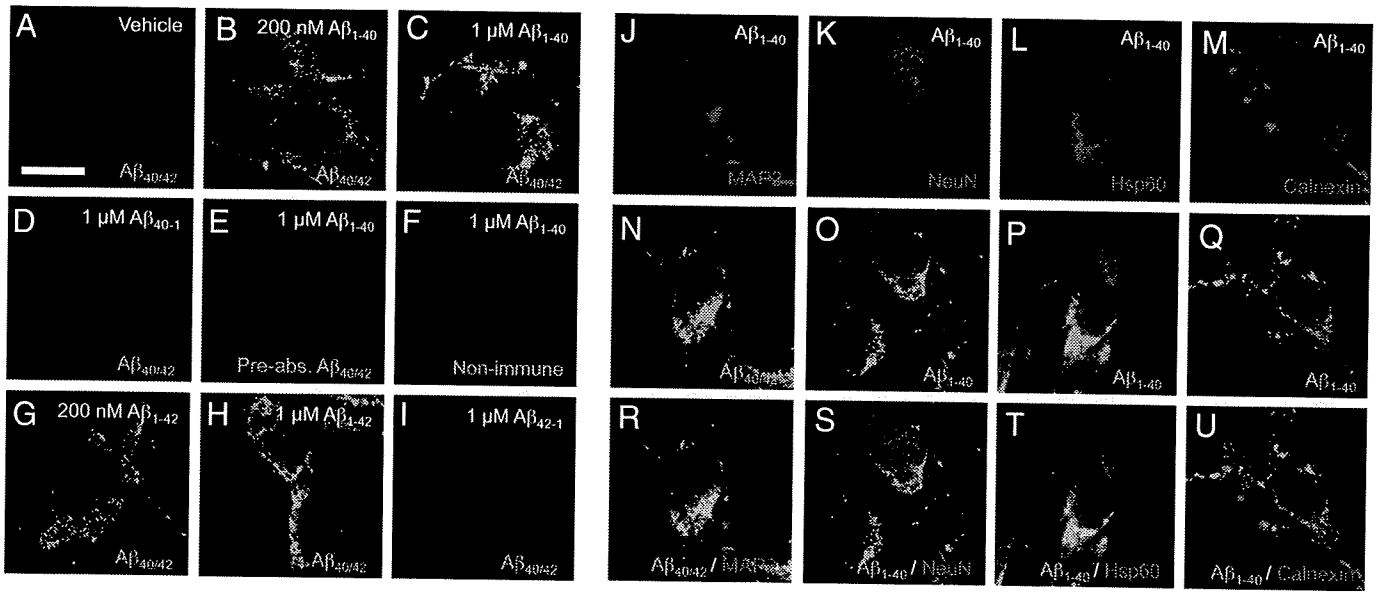

Fig. 1. Confocal images of Aβ, MAP2, NeuN, Hsp60, and calnexin in cortical neurons after exposure to Aβ-related peptides. Cells were exposed to the indicated concentration [or 1 μM (*J–U*)] of human $A\beta_{1-40}$, $A\beta_{1-42}$, reversed Aβ ($A\beta_{40-1}$ and $A\beta_{42-1}$), or vehicle for 60 min, fixed in 3% PFA, and stained by [anti-human Aβ (clone 4G8) (*A–D*, *G–I*, *N*, and *R*), anti-$A\beta_{1-40}$ (*O–P* and *S–U*), preabsorbed anti-Aβ (clone 4G8) (*E*) or non-immune IgG (*F*)]/Alexa Fluor 488 anti-IgG (green), anti-MAP2/Alexa Fluor 568 anti-IgG (red) (*J* and *R*) and [anti-NeuN (*K* and *S*), anti-Hsp 60 (*L* and *T*), or anti-calnexin (*M* and *U*)]/Alexa Fluor 546 anti-IgG (red). Scale bar, 10 μm. Hoechst 33342 staining and phase contrast images of the same field of cells in panels of *A*, *C*, *H*, *D*, or Fig. S4 *A–D* are represented in Fig. S4 *E–H* and *M–P*, respectively.

suggested the possibility that Aβ added to the extracellular milieu gained access to the intracellular space and, subsequently, interacted with its intracellular target. These findings led us to probe mechanisms through which Aβ gains access to intracellular compartments.

To evaluate cellular uptake of Aβ, we first measured levels of intracellular Aβ in neurons treated with the synthetic human Aβ peptides by ELISA using an antibody specific for the human form of Aβ to differentiate it from endogenous mouse Aβ. To remove Aβ bound to the cell surface, cells were treated with trypsin for 5 min before harvest for measurement of the intracellular human Aβ. As shown in Figs. S2 and S3, intracellular human Aβ content was at background levels in vehicle-treated neurons, whereas levels of intracellular human Aβ were significantly increased in mouse cortical neurons incubated with human $A\beta_{1-40}$ and $A\beta_{1-42}$. The accumulation of both $A\beta_{1-40}$ and $A\beta_{1-42}$ peptides occurred in a time- (Figs. S2*A* and *B* and S3*A* and *C*) and dose-dependent (Figs. S2*C* and S3 *A* and *C*) manner. Biochemical subcellular fractionation further revealed that the majority of the intracellular Aβ was detected in the mitochondria-enriched fractions (Fig. S3*F*) as compared with plasma membrane (Fig. S3*E*) and cytosolic fractions (Fig. S3*G*). As a complementary approach, we performed confocal microscopy using double immunofluorescence with antibodies to Aβ and intracellular markers, such as MAP-2 (neuronal marker), NeuN (neuronal marker), Hsp60 (mitochondrial marker), and calnexin (endoplasmic reticulum marker). After exposure (60 min) to human $A\beta_{1-40}$ and $A\beta_{1-42}$, but not $A\beta_{40-1}$ (Fig. 1*H*) and $A\beta_{42-1}$ (Fig. 1*I*), neurons displayed immunoreactivity to anti-human Aβ antibody (clone 4G8) in a cytosolic-like distribution, in addition to a cell surface-like staining pattern (Fig. 1 *B*, *C*, *G*, and *H*; double staining images with Hoechst 33342, Fig. S4 *J* and *K*). In contrast, immunoreactivity to anti-human Aβ antibody (clone 4G8) preabsorbed with $A\beta_{1-40}$ (Fig. 1*E*) or to non-immune serum (Fig. 1*F*), was background level in the cells exposed to human $A\beta_{1-40}$. Cells without Aβ treatment also showed no specific staining patterns (Fig. 1*A*). Intracellular $A\beta_{1-40}$ was observed in cells stained positively for two neuronal markers, MAP2 (Fig. 1*R*) and NeuN (Fig. 1*S*). Further analysis using the mitochondrial marker Hsp60 demonstrated extensive colocalization with Aβ epitopes (Fig. 1*T*), although to a lesser extent with the endoplasmic reticulum marker calnexin (Fig. 1*U*). To confirm localization of Aβ to the intracellular space, we performed immunogold electron microscopy on cultured neurons. Immunogold particles labeled Aβ and were present in the intracellular space, such as the cytosolic compartment and mitochondria, after exposure of neurons to $A\beta_{1-42}$. In contrast, the number of immunogold particles was significantly diminished in RAGE-deficient ($RAGE^{-/-}$) neurons (Fig. 2*C*), as compared with wild-type (WT) neurons (Fig. 2 *A* and *B*). Gold particles were virtually absent when cells were treated with vehicle alone (without treatment of Aβ, Fig. S5 *A* and *B*) or $A\beta_{1-42}$ antibody was replaced by non-immune IgG (Fig. S5 *C* and *D*). Quantification of the total number of gold particles per field, based on analysis of multiple images, confirmed a significant decrease Aβ-immunogold particles in $RAGE^{-/-}$ neurons as compared with WT neurons (Fig. 2*D*). These data suggest that exogenous Aβ gains access to intracellular compartments, such as mitochondria, and that absence of RAGE reduces Aβ transport to the intracellular compartment. Neurons exposed to 1 μM $A\beta_{1-42}$ (Fig. S6, part 1) and lower concentration (200 nM) of $A\beta_{1-40}$ (Fig. S6, part 2) showed a similar intracellular distribution of the peptide.

Blockade of RAGE Diminishes Aβ Uptake and Aβ-Induced Mitochondrial Dysfunction. To determine the potential role of RAGE in neuronal Aβ transport, the effect of a blocking antibody to the receptor on Aβ uptake and neurotoxicity was examined in mouse cortical neuron cultures. Pretreatment of neuronal cultures with anti-RAGE IgG (N-16) for 2 h attenuated uptake of human $A\beta_{1-40}$ (Fig. 3*A*) and $A\beta_{1-40}$-induced mitochondrial dysfunction, at the level of MTT reduction (Fig. S7*A*). In contrast, non-immune IgG had no effect on either uptake of Aβ or MTT reduction. To further examine RAGE-dependent neuronal Aβ transport, neurons prepared from $RAGE^{-/-}$ mice were used. Neurons lacking RAGE showed a marked decrease in uptake of $A\beta_{1-40}$ (Fig. 3*B*) and complete preservation of MTT reduction in the presence of $A\beta_{1-40}$ (Fig. S7*B*). To examine the effect of RAGE on Aβ-induced mitochondrial dysfunction, we measured mitochondrial respiratory

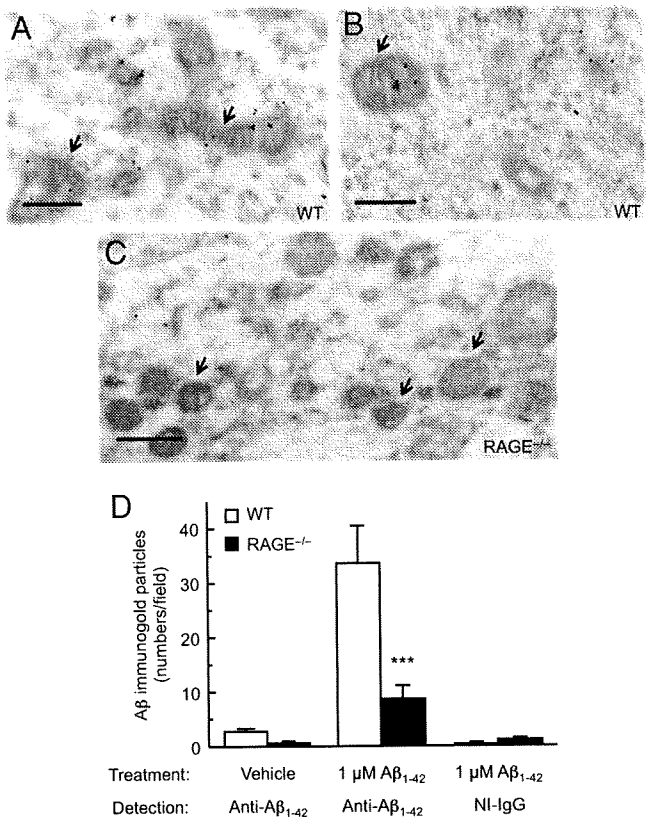

Fig. 2. Immunoelectron microscopy of Aβ in cortical neurons after exposure to Aβ. Cells were prepared from wild-type (WT) (*A* and *B*) and RAGE$^{-/-}$ mice (*C*), exposed to human 1 μM $A\beta_{1-42}$ for 60 min, fixed in 4% PFA and 0.1% glutaraldehyde, and the ultra-thin sections were stained with rabbit anti-$A\beta_{1-42}$/donkey anti-rabbit IgG conjugated to colloidal gold (18 nm particle). Arrows denote mitochondria. (Scale bar, 200 nm.) Two negative controls, in which cells were treated with vehicle or stained with non-immune IgG (NI-IgG), are represented in Fig. S5. (*D*) Quantification of Aβ immunogold particles in WT and RAGE$^{-/-}$ neurons after exposure to Aβ. Numbers of gold particles were counted per field of each microscopic image including two negative controls and expressed as mean ± SEM; ***, $P < 0.001$, versus WT; Unpaired *t*-test.

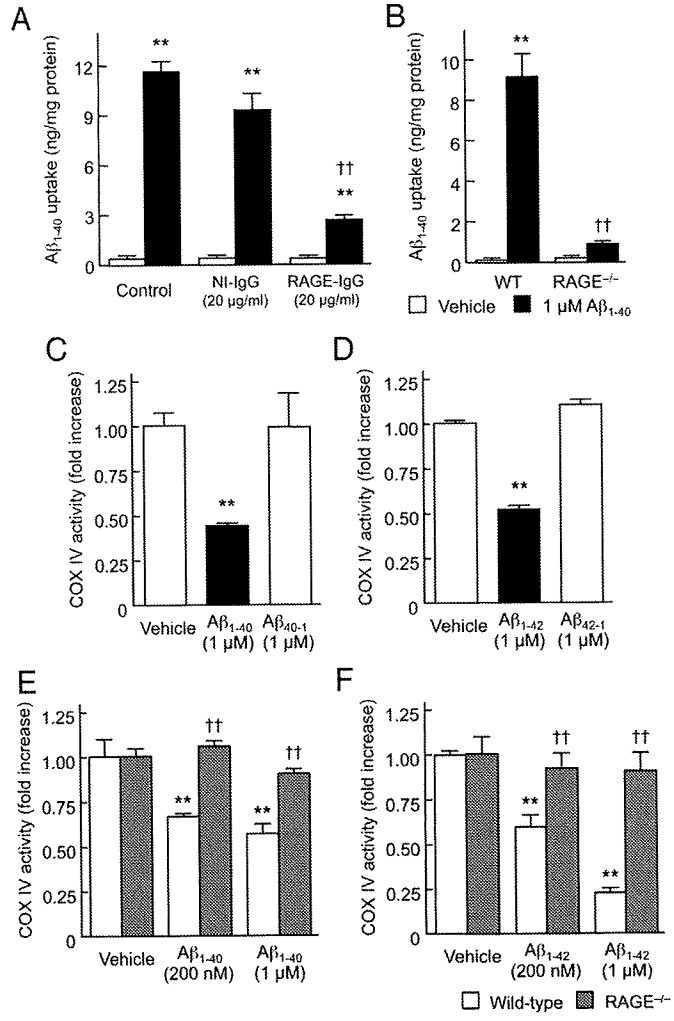

Fig. 3. Blocking RAGE or genetic deletion of the receptor suppresses Aβ uptake and minimizes Aβ-induced mitochondrial dysfunction in cortical neurons. Intracellular levels of human $A\beta_{1-40}$ (*A* and *B*) and COX IV activity (*C–F*) were assayed 60 min (*A* and *B*) and 24 h (*C–F*) after exposure to the indicated Aβ peptides. (*A*) Effect of a neutralizing antibody to RAGE. Cells were pretreated with 20 μg/mL of anti-RAGE (N-16) IgG or NI-IgG for 2 h, and then exposed to 1 μM human $A\beta_{1-40}$. (*B*, *E*, and *F*) Effect of genetic deletion of RAGE. Cells prepared from WT or RAGE$^{-/-}$ mice were exposed to the indicated concentrations of human $A\beta_{1-40}$ (*B* and *E*) or $A\beta_{1-42}$ (*F*). (*C* and *D*) Aβ-related peptides with the reverse sequence have no effect on mitochondrial function in cortical neurons. Cells prepared from wild-type mice were exposed to 1 μM human $A\beta_{1-40}$ or $A\beta_{40-1}$ (*C*), and 1 μM human $A\beta_{1-42}$ or $A\beta_{42-1}$ (*D*). Data represent mean ± SEM; **, $P < 0.01$, versus vehicle- and reversed Aβ-treated cells (*A–D*), or Aβ-treated RAGE$^{-/-}$ neurons (*E* and *F*); ††, $P < 0.01$, versus control (*A* and *B*) or WT (*E* and *F*).

key enzyme cytochrome *c* oxidase (COX IV) activity in RAGE-deficient neurons as compared with COX IV activity in WT neurons. After exposure (24 h) to human $A\beta_{1-40}$ (Fig. 3 *C* and *E*) and $A\beta_{1-42}$ (Fig. 3 *D* and *F*), but not their reversed sequence peptides, neurons displayed a significant dose-dependent reduction in COX IV activity. Notably, RAGE deficiency completely reversed the $A\beta_{1-40}$- and $A\beta_{1-42}$-induced reduction in COX IV activity (Fig. 3 *E* and *F*), which is in agreement with the results of MTT reduction activity. These data indicate that RAGE contributes to transport of Aβ from the cell membrane to the intracellular space, and subsequent induction of mitochondrial dysfunction.

Aβ/RAGE-Mediated Signaling Contributes to Aβ Transport and Internalization. In many contexts, RAGE appears to function as a signal transduction receptor, activating multiple downstream intracellular pathways (22, 31). Thus, we sought to determine if RAGE-mediated cellular activation of such intracellular mechanisms might impact on neuronal Aβ transport. We started by examining the effect of Aβ treatment on phosphorylation of SAPK/JNK and p38 MAPK. Exposure of neurons to $A\beta_{1-40}$ for 10 min did not affect levels of total or phosphorylated forms of SAPK/JNK (Fig. S8*A*). In contrast, neurons exposed to $A\beta_{1-40}$ displayed a dose-dependent increase in phosphorylated p38 MAPK as compared to vehicle-treated controls (Fig. 4 *A* and *D*), although $A\beta_{1-40}$ did not affect total protein levels of p38 MAPK (Fig. 4*A*). $A\beta_{1-42}$ also stimulated p38 MAPK phosphorylation in a similar dose-dependent manner (Fig. S8*B*). Activation of p38 MAPK was observed immediately after $A\beta_{1-40}$ treatment and for up to 30 min (Fig. 4*E*). Pretreatment of neuronal cultures with the p38 MAPK inhibitor SB203580 blocked $A\beta_{1-40}$-stimulated p38 MAPK phosphorylation (Fig. 4*B*). Consistent with these data, neurons pretreated with SB203580, but not a SAPK/JNK inhibitor (SP600125), showed strong inhibition of $A\beta_{1-40}$ uptake (Fig. 4*F*) and MTT reduction in response to $A\beta_{1-40}$ (Fig. S8*C*). A role for RAGE in Aβ-mediated activation of p38 MAPK was indicated by inhibition of p38 phosphorylation in cortical neurons from wild-type mice exposed to Aβ in the presence of anti-RAGE IgG (N-16) (Fig. 4*B*) and in RAGE-deficient cortical neurons derived from RAGE$^{-/-}$ mice (Fig. 4*C*).

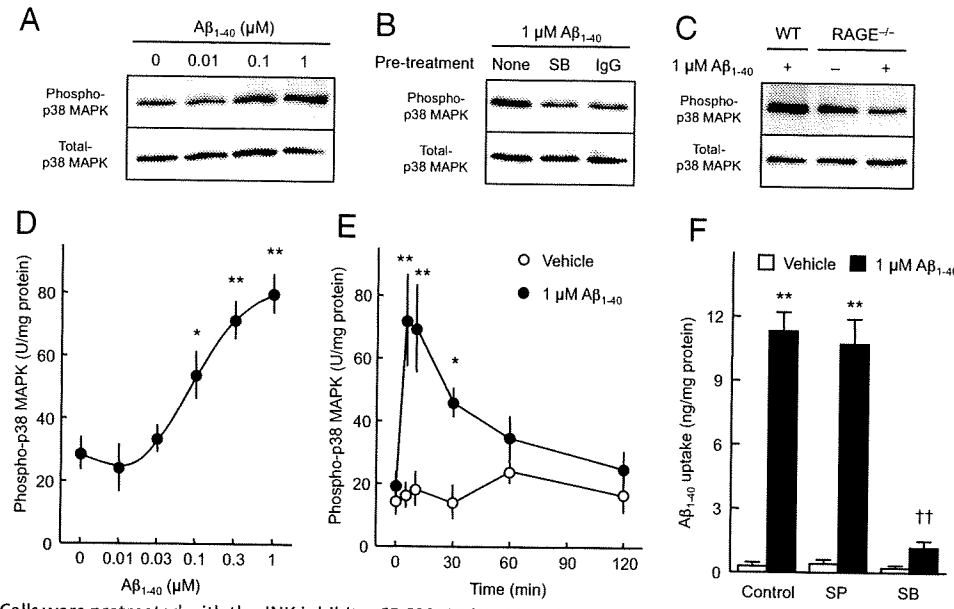

Fig. 4. Aβ-stimulated p38 MAPK activation is required for Aβ uptake in cortical neurons. (*A–C*) Immunoblot analyses of phospho-p38 MAPK in cortical neurons treated with $A\beta_{1-40}$. Cells were exposed to the indicated concentrations of human $A\beta_{1-40}$ for 10 min, lysed, and subjected to SDS/PAGE. Typical immunoblot images detected by antibodies against phospho-p38 MAPK (*A–C*, upper) and total-p38 MAPK (*A–C*, lower) are shown from 3–6 independent experiments. (*A*) Dose-dependency. (*B*) The p38 MAPK inhibitor SB 203580 (1 μM; SB) and anti-RAGE (N-16) IgG (20 μg/mL; IgG) were added 30 min and 2 h before exposure to $A\beta_{1-40}$, respectively. (*C*) Phospho-p38 MAPK levels in neurons from $RAGE^{-/-}$ mice after exposure to $A\beta_{1-40}$. WT, wild-type. (*D* and *E*) Phospho-p38 MAPK levels were determined by ELISA. (*D*) Dose-dependency. Cells were exposed to the indicated concentration of human $A\beta_{1-40}$ for 10 min. (*E*) Time course. Cortical neurons were exposed to 1 μM of human $A\beta_{1-40}$ for the indicated time. (*G*) Effects of JNK and p38 MAPK inhibitors on intracellular levels of human $A\beta_{1-40}$ in cultured neurons exposed to Aβ. Cells were pretreated with the JNK inhibitor SP 600125 (SP, 20 μM), or SB 203580 (SB, 1 μM), for 30 min, and then exposed to 1 μM human $A\beta_{1-40}$ for 60 min. Intracellular $A\beta_{1-40}$ concentrations were determined by ELISA. Data represent mean ± SEM; *, $P < 0.05$, **, $P < 0.01$, versus none (0 μM $A\beta_{1-40}$) (*D* and *F*) and 0-time (*E*); ††, $P < 0.01$, versus control (no inhibitor).

Membrane RAGE Acts as an Aβ Carrier and Co-Internalizes with Aβ. To determine molecular mechanisms underlying neuronal Aβ transport, we biotinylated neuronal cell surface proteins, incubated the labeled cells with $A\beta_{1-40}$, and then analyzed internalized biotinylated proteins. First, we assessed the distribution of biotin in labeled cells before Aβ treatment. Cells fixed immediately after biotinylation and permeabilized with detergent displayed a cell surface and focal [the latter were probably surface accumulations of biotin since they were removed by sodium 2-mercaptoethanesulfonate (MesNa) treatment; see below] distribution of the biotin (Fig. S9*D*) and, as expected, the absence of Aβ (Fig. S9 *A* and *G*). Next, we examined the intracellular distribution of biotin and Aβ in the cells after Aβ treatment. After biotinylation, cells were incubated with vehicle or $A\beta_{1-40}$ for 60 min, treated with MesNa (the latter to remove biotin remaining on the cell surface), fixed and permeabilized with detergent. Cells exposed to $A\beta_{1-40}$ displayed an overlapping intracellular distribution of Aβ (Fig. S9 *C* and *I*) and biotinylated-proteins (Fig. S9 *F* and *I*), while control cells treated with vehicle alone showed no specific signal (Fig. S9 *B*, *E*, and *H*), suggesting that Aβ is able to interact with cell surface proteins.

To analyze internalized proteins in cells exposed to Aβ, we performed Western blotting. After biotinylation of surface proteins, cells were incubated with vehicle or $A\beta_{1-40}$ for 60 min, treated with MesNa, and then whole cell lysates were collected and subjected to immunoprecipitation. Cell lysates contained same amount of total protein, in each case and from both groups, and were reacted with streptavidin followed by SDS/PAGE. Silver staining of gels revealed a broad array of protein bands, especially in cells exposed to $A\beta_{1-40}$, compared with controls (Fig. S10*A*). Interestingly, immunoblotting with anti-RAGE IgG demonstrated >8-fold more RAGE antigen had been immunoprecipitated from cells exposed to $A\beta_{1-40}$, compared with non-treated control (Fig. S10*B*). To determine whether RAGE and Aβ were in the cytosol, we performed immunoprecipitation with anti-Aβ IgG-conjugated beads using the cytosolic fraction from neurons exposed to Aβ. Such cytosolic fractions were obtained by ultracentrifugation (13, 32) and showed virtually undetectable levels of the membrane marker Na^+/K^+-ATPase, compared with presence of the latter in whole cell lysates or membrane-enriched fractions (Fig. S10*C*). Immunoprecipitation analysis was also applied to cytosolic fractions using anti-Aβ IgG-conjugated beads or non-IgG-conjugated beads as a control for nonspecific binding. SDS/PAGE of these immunopreciptates was followed by immunoblotting with anti-RAGE IgG. While there was only a weak signal with immune precipitates prepared in the presence of non-IgG beads, the immune precipitates prepared with anti-Aβ IgG beads demonstrated a strong immunoreactive RAGE band (Fig. S10*D*). Based on image analysis, there was >4-fold more RAGE antigen detected in the immune precipitates with anti-Aβ IgG beads compared with non-IgG beads. These data are consistent with the hypothesis that Aβ stimulates internalization of RAGE, and that during this process, RAGE and Aβ interact closely.

To further assess possible colocalization of RAGE and Aβ, and the spatial topography of these two molecules after internalization of Aβ, we performed dual fluorescence confocal microscopy. Incubation of $A\beta_{1-40}$ with neurons for 60 min demonstrated extensive colocalization of epitopes visualized with anti-RAGE and anti-Aβ antibodies (Fig. S11).

Aβ Colocalizes with RAGE in Hippocampus of Aged Tg-mAPP Mice. To extrapolate these findings to the in vivo setting, we turned to a mouse model of AD-like pathology, transgenic mice overexpressing the human APP isoforms (APP695 and APP751/770) with the familial Alzheimer's dementia mutation (Tg mAPP) and Aβ. Immunohistochemical studies were performed to colocalize intracellular Aβ and RAGE in brains from 9- to 10-month-old mice after permeabilizing the cell membrane with detergent. Compared with wild-type controls (Fig. S12 *A* and *C*), low power immunofluorescence images of brain sections from aged Tg mAPP mice displayed increased staining for Aβ (Fig. S12*B*) and RAGE (Fig. S12*D*) antigens in the hippocampus, especially in the pyramidal cell layer. Plaques in Tg mAPP mice displayed strong staining for Aβ (Fig. S12*B*). High power confocal immunofluorescence images of the hippocampal CA3 region in Tg mAPP mice further demonstrated that Aβ and RAGE co-localized in an apparently intracellular distribution in pyramidal cells (Fig. S12 *F*, *H*, and *J*).

Discussion

Our studies address a paradigm in which Aβ binding to cell surface RAGE translocates the ligand into the cytosolic compartment. Our in vitro studies show that: (*i*) exogenous Aβ translocates from the cell surface to the cytosol, with at least

some of the peptide eventually localizing in mitochondria; (*ii*) such translocation is dependent on RAGE, as it is prevented by blocking antibodies to the receptor and does not occur to an appreciable extent in neurons devoid of RAGE (from $RAGE^{-/-}$ mice); (*iii*) RAGE-mediated cellular activation at the level of p38 MAPK has a central role in internalization of the receptor-ligand complex; and, (*iv*) the presence of Aβ within the cytosol and mitochondria is associated with functional consequences, including mitochondrial dysfunction. Immunoprecipitation of cytosolic fractions after Aβ treatment showed that RAGE itself interacts closely with Aβ, consistent with the concept that the receptor may be the actual Aβ transporter/carrier. As a counterpart to these observations in cell culture, immunohistochemical studies showed colocalization of Aβ and RAGE in an apparently intracellular distribution in hippocampal pyramidal cells in the brains of AD-type transgenic mice expressing mAPP/Aβ.

Increasing evidence points to a role for intraneuronal Aβ in the pathogenesis of early neural dysfunction and AD pathology. Several observations have indicated that APP localizes not only to the plasma membrane, but also to the trans-Golgi network, endoplasmic reticulum, and endosomal, lysosomal, and mitochondrial membranes (5, 7, 33). Thus, two possible pathways could underlie the accumulation of intraneuronal Aβ: (*i*) Aβ secreted into extracellular space is subsequently taken up by neurons (and/or other cells); and, (*ii*) Aβ produced intracellularly remains within the neuron. Our results provide insight into the former pathway, which involves neuronal internalization of both $Aβ_{1-40}$ and $Aβ_{1-42}$. Initially, based on in vitro studies, it was thought that $Aβ_{1-42}$ was more neurotoxic than $Aβ_{1-40}$, in part because of the propensity of $Aβ_{1-42}$ to form large aggregates and fibrils. However, more recently, it has been appreciated that oligomeric and prefibrillar $Aβ_{1-40}$ and $Aβ_{1-42}$ have similar cytotoxic effects (34) and such soluble forms of Aβ are believed to play a critical role in the pathogenesis of AD. Recent work has demonstrated that oligomeric $Aβ_{1-42}$, at a concentration of 200 nM, is capable of blocking long-term potentiation at cortical synapses in the hippocampus and entorhinal cortex (10, 28, 35, 36). Taken together, our findings suggest that via RAGE, neuronal transmembrane transport of $Aβ_{1-40}$ and $Aβ_{1-42}$ carries soluble assemblies of amyloid peptide into the cell.

The present study revealed that intraneuronal accumulation of Aβ could be sustained during exposure to the peptide, especially in mitochondria, as previously reported (10, 12, 37–40). Considerable studies over the past decade have emerged indicating that some intracellular enzymes, insulin-degrading enzyme, endothelin-converting enzyme (ECE)-1b and ECE-2, as well as membrane enzymes, such as neprilysin, ECE-1a, ECE-1c, ECE-1d, matrix metalloproteinase (MMP)-2, MMP-3, and MMP-9, can cleave Aβ at either a single or multiple sites and cleavage products of Aβ resulting from such catabolism are less likely to aggregate and are less neurotoxic than Aβ itself (41). Moreover, a mitochondrial peptidase, PreP peptidasome, has been recently shown to be capable of degrading Aβ (42). As these various amyloid-degrading enzymes have distinct subcellular localization, Aβ metabolism may influence the subcellular accumulation of Aβ and its neurotoxicity. The mechanism through which intraneuronal Aβ is metabolized will require further study to elucidate.

Recent studies demonstrate that several plasma membrane receptors, such as *N*-methyl-D-aspartate receptors (14), α7 nicotinic acetylcholine receptors (15), and low-density lipoprotein receptor-related proteins (LRP) (16), have the capacity to bind to Aβ and, potentially, promote intracellular accumulation of Aβ. Previous studies have shown that RAGE binds monomeric, oligomeric, and even fibrillar forms of Aβ at the neuronal cell surface (22, 27, 43). Moreover, RAGE promotes Aβ-induced neuronal dysfunction in a mouse model of AD-type pathology (28). Subsequent to Aβ binding to RAGE on the cell surface, we have found that the amyloid peptide is internalized in a RAGE-dependent manner; blocking RAGE or deletion of the receptor attenuates Aβ internalization and Aβ-induced mitochondrial dysfunction in cortical neurons. These findings strongly suggest a role for RAGE as a cell surface-binding site and a potential transporter for Aβ which facilitates intracellular transfer of the peptide.

RAGE-ligand interaction has been shown to activate multiple intracellular signaling pathways including the MAPKs (ERK1/2, p38 MAPK and SAPK/JNK), rho-GTPases, phosphoinositol-3-kinase, and the JAK/STAT pathway in various cells (23, 43). In addition, the RAGE-ligand interaction has been shown to directly cause generation of reactive oxygen species via NADPH oxidases (44). As a consequence of Aβ–RAGE interaction, activation of p38 MAPK, SAPK/JNK, and NF-κB was observed in sporadic AD cybrids (45). In addition, Arancio et al. (28) reported increased phosphorylation of CREB, ERK1/2, p38 MAPK, and CaMKII in hippocampal extracts from Tg mice overexpressing RAGE and mAPP. RAGE-dependent activation of p38 signal transduction also plays an important role in Aβ-mediated synaptic failure (35, 36). However, direct links between RAGE-mediated signaling pathways and Aβ neurotoxicity remain to be fully elucidated. The present study indicates that the Aβ-RAGE interaction rapidly activates p38 MAPK, but not SAPK/JNK, and further demonstrates a link between activation of p38, intracellular Aβ accumulation, and Aβ-induced cytotoxicity in cortical neurons.

In the BBB endothelial cells, RAGE and LRP1 have shown to be critical for regulation of Aβ homeostasis in the central nervous system (46). RAGE binds soluble Aβ at the apical side of human BBB, and promotes transport of soluble Aβ from blood to brain via endocytosis and transcytosis. These events promote Aβ accumulation in brain parenchyma (29, 47). Our biotinylation study revealed that Aβ stimulated internalization of neuronal plasma membrane proteins, including RAGE, and that RAGE–Aβ complex was present intracellularly. These finding suggest that the interaction of Aβ with RAGE activates an endocytosis-like pathway that causes rapid internalization of Aβ–RAGE complex. Consistent with these in vitro results, recent studies in brains of AD patients (48) and another mouse AD model (49) displayed striking accumulation of Aβ in hippocampal pyramidal cells.

In conclusion, our study demonstrates that Aβ induces a RAGE-dependent pathway that involves activation of p38 MAPK, resulting in internalization of Aβ and leading to mitochondrial dysfunction in cultured cortical neurons. We propose that Aβ internalization may be associated with RAGE-mediated endocytosis and that RAGE itself may act as a carrier in transmembrane Aβ transport. The mechanism through which Aβ gains access to the cytosol and enters mitochondria will require further study to elucidate. Cytosolic Aβ may enter mitochondria through the TOM pathway as recently reported (39) leading to mitochondrial stress. The results of our studies contribute to a growing body of evidence demonstrating that RAGE can act as a receptor magnifying intraneuronal Aβ cytotoxicity. Blockade of RAGE may have a beneficial effect by limiting intracellular accumulation of amyloid in AD brain and serves a potential therapeutic target for AD.

Materials and Methods

For full description of this study's materials and methods, see *SI Materials and Methods*.

Animals. RAGE knockout ($RAGE^{-/-}$) mice have been described previously (35, 50).

Cell Culture. Cortical neurons were prepared from embryos at 17 days of gestation of C57BL/6J mice, transgenic mice overexpressing the human full-length ABAD (Tg-ABAD mice) and homozygous $RAGE^{-/-}$ mutant mice.

Biochemical Determination of Neuronal Perturbation. Neuronal perturbation after Aβ treatment was determined by generation of reactive oxygen species (ROS), mitochondrial membrane potential, caspase activity, DNA fragmentation, MTT reduction, and cytochrome *c* oxidase (COX IV) activity assays.

Determination of Membrane Aβ Transport. Transport of Aβ into cytosol through the plasma membrane was measured by ELISA and detected by confocal immunofluorescence and immunoelectron microscopies using anti-Aβ IgG.

Measurement of Phospho-MAPKs. Aβ-stimulated phosphorylation of SAPK/JNK and p38 MAPK was detected by Western blot analysis or measured by ELISA.

Analysis of Internalization of Membrane Surface Proteins. Internalization of membrane surface proteins after Aβ treatment was detected by Western blot analysis using biotinylation and immunoprecipitation.

Immunohistochemistry. Immunohistochemistry was executed in hippocampal sections from Tg mAPP mice (9- to 10-month-old) and age- and strain-matched wild-type mice using anti-Aβ IgG and anti-RAGE IgG.

Statistics. Statistical analysis of the experimental data were carried out using GraphPad Prism 4 for Macintosh (GraphPad Software). The significance of differences was determined by a one-way ANOVA, followed by the Dunnett's or Tukey's multiple comparison test for multigroup comparisons. Unpaired *t*-test was used for two-group comparisons. The criterion for statistical significance was $P < 0.05$.

ACKNOWLEDGMENTS. This study was supported in part by a grant for the 21st Century Centers of Excellence Program (1640102) from the Ministry of Education, Culture, Sports, Science and Technology of Japan, a Grant-in-Aid for Scientific Research (18590050) from the Japan Society for the Promotion of Science, and a grant from Takeda Science Foundation. This work was also supported by grant from the U.S. Public Health Service (PO1AG17490).

1. Yankner BA (1996) Mechanisms of neuronal degeneration in Alzheimer's disease. *Neuron* 16:921–932.
2. LaFerla FM, Oddo S (2005) Alzheimer's disease: Aβ, tau, and synaptic dysfunction. *Trends Mol Med* 11:170–176.
3. Gouras GK, et al. (2000) Intraneuronal Aβ42 accumulation in human brain. *Am J Pathol* 156:15–20.
4. Takahashi RH, et al. (2002) Intraneuronal Alzheimer Aβ42 accumulates in multivesicular bodies and is associated with synaptic pathology. *Am J Pathol* 161:869–879.
5. LaFerla FM, Green KN, Oddo S (2007) Intracellular amyloid-β in Alzheimer's disease. *Nat Rev Neurosci* 8:499–509.
6. Reddy PH, Beal MF (2008) Amyloid β, mitochondrial dysfunction and synaptic damage: Implications for cognitive decline in aging and Alzheimer's disease. *Trends Mol Med* 14:45–53.
7. Lin MT, Beal MF (2006) Alzheimer's APP mangles mitochondria. *Nat Med* 12:1241–1243.
8. Chen X, Stern D, Yan SD (2007) in *Neurobiology of Alzheimer's Disease*, eds Dawbarn D, Allen SJ (Oxford Univ. Press, New York), 3rd Ed, pp 227–244.
9. Caspersen C, et al. (2005) Mitochondrial Aβ: A potential focal point for neuronal metabolic dysfunction in Alzheimer's disease. *FASEB J* 19:2040–2041.
10. Du H, et al. (2008) Cyclophilin D deficiency attenuates mitochondrial and neuronal perturbation and ameliorates learning and memory in Alzheimer's disease. *Nat Med* 14:1097–1105.
11. Du H, Guo L, Zhang W, Rydzewska M, Yan S (2009) Cyclophilin D deficiency improves mitochondrial function and learning/memory in aging Alzheimer disease mouse model. *Neurobiol Aging*, in press.
12. Lustbader JW, et al. (2004) ABAD directly links Aβ to mitochondrial toxicity in Alzheimer's disease. *Science* 304:448–452.
13. Takuma K, et al. (2005) ABAD enhances Aβ-induced cell stress via mitochondrial dysfunction. *FASEB J* 19:597–598.
14. Snyder EM, et al. (2005) Regulation of NMDA receptor trafficking by amyloid-β. *Nat Neurosci* 8:1051–1058.
15. Nagele RG, D'Andrea MR, Anderson WJ, Wang HY (2002) Intracellular accumulation of β-amyloid$_{1-42}$ in neurons is facilitated by the α7 nicotinic acetylcholine receptor in Alzheimer's disease. *Neuroscience* 110:199–211.
16. Zerbinatti CV, et al. (2006) Apolipoprotein E and low density lipoprotein receptor-related protein facilitate intraneuronal Aβ42 accumulation in amyloid model mice. *J Biol Chem* 281:36180–36186.
17. Cardoso SM, Santana I, Swerdlow RH, Oliveira CR (2004) Mitochondria dysfunction of Alzheimer's disease cybrids enhances Aβ toxicity. *J Neurochem* 89:1417–1426.
18. Ren Y, et al. (2008) Endophilin I expression is increased in the brains of Alzheimer disease patients. *J Biol Chem* 283:5685–5691.
19. Yao J, et al. (2007) Interaction of amyloid binding alcohol dehydrogenase/Aβ mediates up-regulation of peroxiredoxin II in the brains of Alzheimer's disease patients and a transgenic Alzheimer's disease mouse model. *Mol Cell Neurosci* 35:377–382.
20. Neeper M, et al. (1992) Cloning and Expression of a cell surface receptor for advanced glycosylation end products of proteins. *J Biol Chem* 267:14998–15004.
21. Schmidt AM, et al. (1992) Isolation and characterization of two binding proteins for advanced glycosylation end products from bovine lung which are present on the endothelial cell surface. *J Biol Chem* 267:14987–14997.
22. Chen X, et al. (2007) RAGE: A potential target for Aβ-mediated cellular perturbation in Alzheimer's disease. *Curr Mol Med* 7:735–742.
23. Bucciarelli LG, et al. (2002) RAGE is a multiligand receptor of the immunoglobulin superfamily: Implications for homeostasis and chronic disease. *Cell Mol Life Sci* 59:1117–1128.
24. Bierhaus A, et al. (2005) Understanding RAGE, the receptor for advanced glycation end products. *J Mol Med* 83:876–886.
25. Yan SD, et al. (1996) RAGE and amyloid-β peptide neurotoxicity in Alzheimer's disease. *Nature* 382:685–691.
26. Yan SD, et al. (1995) Nonenzymatically glycated tau in Alzheimer's disease induces neuronal oxidant stress resulting in cytokine gene expression and release of Aβ. *Nat Med* 1:693–699.
27. Lue LF, et al. (2001) Involvement of microglial receptor for advanced glycation end-products (RAGE) in Alzheimer's disease: Identification of a cellular activation mechanism. *Exp Neurol* 171:29–45.
28. Arancio O, et al. (2004) RAGE potentiates Aβ-induced perturbation of neuronal function in transgenic mice. *EMBO J* 23:4096–4105.
29. Giri R, et al. (2000) β-Amyloid-induced migration of monocytes across human brain endothelial cells involves RAGE and PECAM-1. *Am J Physiol Cell Physiol* 279:C1772–C1781.
30. Deane R, et al. (2003) RAGE mediates amyloid-β peptide transport across the blood-brain barrier and accumulation in brain. *Nat Med* 9:907–913.
31. Schmidt AM, Yan SD, Yan SF, Stern DM (2001) The multiligand receptor RAGE as a progression factor amplifying immune and inflammatory responses. *J Clin Invest* 108:949–955.
32. Hurt CM, Feng FY, Kobilka B (2000) Cell-type specific targeting of the α_{2c}-adrenoceptor: Evidence for the organization of receptor microdomains during neuronal differentiation of PC12 cells. *J Biol Chem* 275:35424–35431.
33. Anandatheerthavarada HK, Biswas G, Robin MA, Avadhani NG (2003) Mitochondrial targeting and a novel transmembrane arrest of Alzheimer's amyloid precursor protein impairs mitochondrial function in neuronal cells. *J Cell Biol* 161:41–54.
34. Cecchi C, et al. (2007) Increased susceptibility to amyloid toxicity in familial Alzheimer's fibroblasts. *Neurobiol Aging* 28:863–876.
35. Origlia N, et al. (2008) Receptor for advanced glycation end product-dependent activation of p38 mitogen-activated protein kinase contributes to amyloid-β-mediated cortical synaptic dysfunction. *J Neurosci* 28:3521–3530.
36. Origlia N, et al. (2009) Aβ-dependent Inhibition of LTP in different intracortical circuits of the visual cortex: The role of RAGE. *J Alzheimers Dis* 17:59–68.
37. Manczak M, et al. (2006) Mitochondria are a direct site of Aβ accumulation in Alzheimer's disease neurons: Implications for free radical generation and oxidative damage in disease progression. *Hum Mol Genet* 15:1437–1449.
38. Yao J, et al. (2009) Mitochondrial bioenergetic deficit precedes Alzheimer's pathology in female mouse model of Alzheimer's disease. *Proc Natl Acad Sci USA*, in press.
39. Hansson Petersen CA, et al. (2008) The amyloid β-peptide is imported into mitochondria via the TOM import machinery and localized to mitochondrial cristae. *Proc Natl Acad Sci USA* 105:13145–13150.
40. Crouch PJ, et al. (2005) Copper-dependent inhibition of human cytochrome *c* oxidase by a dimeric conformer of amyloid-β$_{1-42}$. *J Neurosci* 25:672–679.
41. Miners JS, et al. (2008) Aβ-degrading enzymes in Alzheimer's disease. *Brain Pathol* 18:240–252.
42. Falkevall A, et al. (2006) Degradation of the amyloid β-protein by the novel mitochondrial peptidasome, PreP. *J Biol Chem* 281:29096–29104.
43. Ding Q, Keller JN (2005) Evaluation of rage isoforms, ligands, and signaling in the brain. *Biochim Biophys Acta* 1746:18–27.
44. Wautier MP, et al. (2001) Activation of NADPH oxidase by AGE links oxidant stress to altered gene expression via RAGE. *Am J Physiol Endocrinol Metab* 280:E685–E694.
45. Onyango IG, Tuttle JB, Bennett JP Jr (2005) Altered intracellular signaling and reduced viability of Alzheimer's disease neuronal cybrids is reproduced by β-amyloid peptide acting through receptor for advanced glycation end products (RAGE). *Mol Cell Neurosci* 29:333–343.
46. Deane R, et al. (2009) Clearance of amyloid-β peptide across the blood-brain barrier: Implication for therapies in Alzheimer's disease. *CNS Neurol Disord Drug Targets* 8:16–30.
47. Mackic JB, et al. (1998) Human blood-brain barrier receptors for Alzheimer's amyloid-β 1–40. Asymmetrical binding, endocytosis, and transcytosis at the apical side of brain microvascular endothelial cell monolayer. *J Clin Invest* 102:734–743.
48. D'Andrea MR, Derian CK, Santulli RJ, Andrade-Gordon P (2001) Evidence that neurones accumulating amyloid can undergo lysis to form amyloid plaques in Alzheimer's disease. *Histopathology* 38:120–134.
49. Oakley H, et al. (2006) Intraneuronal β-amyloid aggregates, neurodegeneration, and neuron loss in transgenic mice with five familial Alzheimer's disease mutations: Potential factors in amyloid plaque formation. *J Neurosci* 26:10129–10140.
50. Sakaguchi T, et al. (2003) Central role of RAGE-dependent neointimal expansion in arterial restenosis. *J Clin Invest* 111:959–972.

Psychopharmacology
DOI 10.1007/s00213-008-1240-6

ORIGINAL INVESTIGATION

Aripiprazole ameliorates phencyclidine-induced impairment of recognition memory through dopamine D_1 and serotonin 5-HT_{1A} receptors

Taku Nagai · Rina Murai · Kanae Matsui · Hiroyuki Kamei · Yukihiro Noda · Hiroshi Furukawa · Toshitaka Nabeshima

Received: 10 March 2008 / Accepted: 13 June 2008

Abstract
Rationale Cognitive deficits, including memory impairment, are regarded as a core feature of schizophrenia. Aripiprazole, an atypical antipsychotic drug, has been shown to improve disruption of prepulse inhibition and social interaction in an animal model of schizophrenia induced by phencyclidine (PCP); however, the effects of aripiprazole on recognition memory remain to be investigated.

Objectives In this study, we examined the effect of aripiprazole on cognitive impairment in mice treated with PCP repeatedly.
Materials and methods Mice were repeatedly administered PCP at a dose of 10mg/kg for 14days, and their cognitive function was assessed using a novel-object recognition task. We investigated the therapeutic effects of aripiprazole (0.01–1.0mg/kg) and haloperidol (0.3 and 1.0mg/kg) on cognitive impairment in mice treated with PCP repeatedly.
Results Single (1.0mg/kg) and repeated (0.03 and 0.1mg/kg, for 7days) treatment with aripiprazole ameliorated PCP-induced impairment of recognition memory, although single treatment significantly decreased the total exploration time during the training session. In contrast, both single and repeated treatment with haloperidol (0.3 and 1.0mg/kg) failed to attenuate PCP-induced cognitive impairment. The ameliorating effect of aripiprazole on recognition memory in PCP-treated mice was blocked by co-treatment with a dopamine D_1 receptor antagonist, SCH23390, and a serotonin 5-HT_{1A} receptor antagonist, WAY100635; however, co-treatment with a D_2 receptor antagonist raclopride had no effect on the ameliorating effect of aripiprazole.
Conclusions These results suggest that the ameliorative effect of aripiprazole on PCP-induced memory impairment is associated with dopamine D_1 and serotonin 5-HT_{1A} receptors.

Keywords Aripiprazole · Dopamine D_1 receptor · Memory · Phencyclidine · Serotonin 5-HT_{1A} receptor

Electronic supplementary material The online version of this article (doi:10.1007/s00213-008-1240-6) contains supplementary material, which is available to authorized users.

T. Nagai · T. Nabeshima
Department of Neuropsychopharmacology and Hospital Pharmacy, Nagoya University Graduate School of Medicine, Nagoya, Japan

R. Murai · T. Nabeshima (✉)
Department of Chemical Pharmacology,
Graduate School of Pharmaceutical Sciences, Meijo University,
150 Yagotoyama, Tenpaku-ku,
Nagoya 468-8503, Japan
e-mail: tnabeshi@ccmfs.meijo-u.ac.jp

K. Matsui · H. Kamei
Department of Health-Care Pharmacy,
Graduate School of Pharmaceutical Sciences, Meijo University,
Nagoya, Japan

Y. Noda
Division of Clinical Science in Clinical Pharmacy Practice,
Graduate School of Pharmaceutical Sciences, Meijo University,
Nagoya, Japan

H. Furukawa
Department of Medical Chemistry,
Graduate School of Pharmaceutical Sciences, Meijo University,
Nagoya, Japan

Introduction

Schizophrenia is a devastating psychiatric disorder that impairs mental and social functioning and affects approx-

imately 1% of the population worldwide (Rössler et al. 2005). Typical symptoms can be separated into positive symptoms (e.g., hallucinations, delusions, and thought disorder), negative symptoms (e.g., deficits in social interaction, emotional expression, and motivation), and cognitive dysfunction (e.g., impaired attention/information processing, problem-solving, processing speed, verbal and visual learning, and memory and working memory) (Nuechterlein et al. 2004; Pearlson 2000). Pharmacological treatment of schizophrenia is available. First-generation (typical) antipsychotics alleviate psychotic symptoms, but lead to severe motor side effects through the blockade of dopamine D_2 receptors (Kapur et al. 2000). Second-generation (atypical) antipsychotics have improved tolerability and milder motor side effects than typical antipsychotics but induce weight gain and metabolic disturbances (Newcomer 2005). Despite appropriate treatment with either typical antipsychotics or atypical antipsychotics, schizophrenic patients continue to exhibit pronounced cognitive impairment (Keefe et al. 2007; Mishara and Goldberg 2004; Woodward et al. 2005).

Aripiprazole, 7-(4-[4-(2,3-dichlorophenyl)-1-piperazinyl] butyloxy)-3,4-dihydro- carbostycil, is a novel atypical antipsychotic drug that differs from other typical and atypical antipsychotics, improving both positive and negative symptoms of psychosis without producing extrapyramidal side effects or increases in serum prolactin (DeLeon et al. 2004; Tamminga 2002). It has been demonstrated that aripiprazole has high affinity for a large number of monoaminergic receptors, including dopamine D_2, serotonin 5-HT_{1A}, and 5-HT_{2A} receptors (Green 2004; Shapiro et al. 2003) and acts as a partial dopamine D_2 receptor agonist (Kikuchi et al. 1995), a partial 5-HT_{1A} receptor agonist (Jordan et al. 2002), and as an 5-HT_{2A} receptor antagonist (McQuade et al. 2002). These pharmacological properties may play a role in the therapeutic effects of aripiprazole. Although aripiprazole has been reported to enhance cognitive function in schizophrenia (Rivas-Vasquez 2003), the mechanism of the improving effect of aripiprazole on cognitive impairment is unclear.

Phencyclidine [1-(1-phenylcyclohexyl) piperidine hydrochloride (PCP)], a noncompetitive *N*-metyl-D-aspartate receptor antagonist, has been shown to induce schizophrenia-like psychosis, presenting as positive symptoms, negative symptoms, and cognitive deficits in humans (Javitt and Zukin 1991), which persist several weeks after withdrawal of chronic PCP use (Allen and Young 1978; Lerner and Burns 1986; Rainey and Crowder 1975). To investigate the pathophysiology of schizophrenia, an animal model of schizophrenia was established using PCP (Mouri et al. 2007a). We have previously demonstrated that repeated treatment with PCP (10mg/kg/day s.c. for 14days) induces several schizophrenia-like behavioral abnormalities, such as increased immobility in a forced swimming test (Murai et al. 2007; Noda et al. 1995, 1997, 2000), social deficits in a social interaction test (Qiao et al. 2001), impairment of latent learning in a water finding test (Mouri et al. 2007b), and associative learning impairment in cued and contextual fear conditioning tests (Enomoto et al. 2005) in mice. Moreover, it has been reported that PCP induces the disruption of sensorimotor gating in a prepulse inhibition test (Bakshi et al. 1994) and recognition memory in a novel object recognition test (Hashimoto et al. 2005); therefore, PCP-treated mice might be a useful animal model of schizophrenia.

There are a few reports suggesting the effectiveness of aripiprazole on cognitive dysfunction and negative symptoms in PCP-treated animals. For example, aripiprazole improves PCP-induced disruption of prepulse inhibition (Fejgin et al. 2007) and social interaction (Bruins Slot et al. 2005) in mice and rats, respectively; however, the effects of aripiprazole on recognition memory remain to be investigated. In this study, we examined whether aripiprazole improves PCP-induced cognitive impairment in a novel object recognition test in mice.

Materials and methods

Animals

Male ICR mice (7weeks old) were obtained from Nihon SLC (Shizuoka, Japan). The animals were housed in plastic cages and kept in a regulated environment (23 ± 1°C, 50 ± 5% humidity), with a 12/12h light–dark cycle (lights on at 09:00hours). Food (CE2; Clea Japan, Tokyo, Japan) and tap water were available ad libitum. All animal care and use were in accordance with the National Institutes of Health Guide for the Care and Use of Laboratory Animals and were approved by the Institutional Animal Care and Use Committee of Nagoya University.

Drugs

PCP hydrochloride was synthesized by the authors according to the method of Maddox et al. (1965) and was checked for purity. Aripiprazole was provided by Otsuka Pharmaceutical (Tokyo, Japan). SCH23390 hydrochloride, *S*-(−)-raclopride (+)-tartrate, haloperidol and WAY100635 were purchased from Sigma-Aldrich (St. Louis, MO, USA). The dose of each drug refers to previous reports (Noda et al. 1995; Bruins Slot et al. 2005; Kamei et al. 2006; Ito et al. 2007b).

PCP was dissolved in saline. SCH23390, raclopride, and WAY100635 was dissolved in distilled water. Aripiprazole and haloperidol were suspended in saline containing 0.1% carboxymethylcellulose (CMC) sodium salt. All drugs were administered in a volume of 0.1ml/10g body weight.

Measurement of locomotor activity

Each mouse was placed in a standard transparent rectangular rodent cage (25 × 30 × 18 high cm). Locomotor activity was then measured for 1h, using an infrared sensor (NS-AS01; Neuroscience, Tokyo, Japan) placed over the cage (Ito et al. 2007a).

Novel object recognition test

The novel object recognition test was performed according to previously reported methods (Nagai et al. 2003; Tang et al. 1999). The experimental apparatus consisted of a Plexiglas open-field box (30 × 30 × 35 high cm), the floor of which was covered in sawdust. The apparatus was located in a sound-attenuated room and illuminated with a 20-W bulb.

The procedure for the novel object recognition test consisted of three different sessions: habituation, training, and retention. Each mouse was individually habituated to the box, with 10min of exploration in the absence of objects each day for three consecutive days (habituation session, days1–3). In the training session, two different novel objects were symmetrically fixed to the floor of the box, 8cm from the walls, and each animal was allowed to explore the box for 10min (day4). The objects were a golf ball, wooden cylinders, and square pyramids, which were different in shape and color but similar in size. An animal was considered to be exploring the object when its head was facing the object or it was touching or sniffing the object. The time spent exploring each object was recorded. After training, mice were immediately returned to their home cages. In the retention sessions, the animals were placed back into the same box 24h (day5) after the training session, but with one of the familiar objects used during training replaced by a novel object. The animals were then allowed to explore freely for 5min, and the time spent exploring each object was recorded. Throughout the experiments, the objects were balanced in terms of their physical complexity and emotional neutrality. A preference index, the ratio of the amount of time spent exploring any one of the two objects (training session) or the novel object (retention session) over the total time spent exploring both objects, was used to measure cognitive function.

Drug treatment

For effect of single treatment on locomotor activity, 0.1% CMC, aripiprazole (0.1–1.0mg/kg) or haloperidol (0.3–1.0mg/kg) was orally (p.o.) administered 1h before the experiment. The number of animals included in each drug treatment was as follows: CMC (n = 12), 0.1mg/kg aripiprazole (n = 12), 0.3mg/kg aripiprazole (n = 12), 1.0mg/kg aripiprazole (n = 11) for Fig. 1b,c; CMC (n = 10), 0.3mg/kg haloperidol (n = 10), 1.0mg/kg haloperidol (n = 10) for Fig. 1d,e.

For effect of repeated treatment on locomotor activity, 0.1% CMC, aripiprazole (0.01–0.1mg/kg), or haloperidol (0.3–1.0mg/kg) was p.o. administered for 7days; the experiment was performed 24h after last treatment. Locomotor activity was recorded for 1h. The number of animals included in each drug treatment was as follows: CMC (n = 10), 0.01mg/kg aripiprazole (n = 10), 0.03mg/kg aripiprazole (n = 10), 0.1mg/kg aripiprazole (n = 10) for Fig. 2b,c; CMC (n = 10), 0.3mg/kg haloperidol (n = 10), 1.0mg/kg haloperidol (n = 10) for Fig. 2d,e.

We have previously demonstrated that repeated treatment with PCP (10mg/kg/day s.c. for 14days) induces several schizophrenia-like behavioral and neurochemical abnormalities in mice (Murai et al. 2007; Noda et al. 1995, 1997, 2000; Qiao et al. 2001; Mouri et al. 2007b; Enomoto et al. 2005). Therefore, in typical experimental conditions, mice were given the same regimen of PCP (10mg/kg, s.c., for 14days, days1–14). Five days after the last treatment with PCP, the novel object recognition test was performed, including habituation (i.e., days19–21), training (i.e., day22), and retention (i.e., day23) sessions.

To study the single effects of antipsychotics, aripiprazole (0.01–1.0mg/kg) or haloperidol (0.3–1.0mg/kg) was administered p.o. (i.e., day22) to mice that had been previously treated with PCP for 14days (day1–14). One hour after treatment with antipsychotics, the training session using the novel object recognition test was conducted. The number of animals included in each drug treatment was as follows: saline + CMC (n = 16), PCP + CMC (n = 14), PCP + 0.01mg/kg aripiprazole (n = 10), PCP + 0.03mg/kg aripiprazole (n = 9), PCP + 0.1mg/kg aripiprazole (n = 8), PCP + 0.3mg/kg aripiprazole (n = 10), PCP + 1.0mg/kg aripiprazole (n = 11) for Fig. 3b,d; saline + CMC (n = 14), PCP + CMC (n = 13), PCP + 0.3mg/kg haloperidol (n = 7), PCP + 1.0mg/kg haloperidol (n = 9) for Fig. 3c,e.

To study the subchronic effects of antipsychotics, aripiprazole (0.01–0.1mg/kg) or haloperidol (0.3–1.0mg/kg) was administered p.o. once a day for seven consecutive days (i.e., days15–21) to mice that had been previously treated with PCP for 14days (days1–14). During habituation session of the novel object recognition test (i.e., days19–21), mice were administered antipsychotics after the habituation session. One day after the last treatment with antipsychotics (i.e., day22), the training session of the novel object recognition test was conducted. The number of animals included in each drug treatment was as follows: saline + CMC (n = 11), PCP + CMC (n = 10), PCP + 0.01mg/kg aripiprazole (n = 11), PCP + 0.03mg/kg aripiprazole (n = 8), PCP + 0.1mg/kg aripiprazole (n = 8) for Fig. 4b,d; saline + CMC (n = 15), PCP + CMC (n = 14), PCP + 0.3mg/kg haloperidol (n = 8), PCP + 1.0mg/kg haloperidol (n = 9) for Fig. 4c,e.

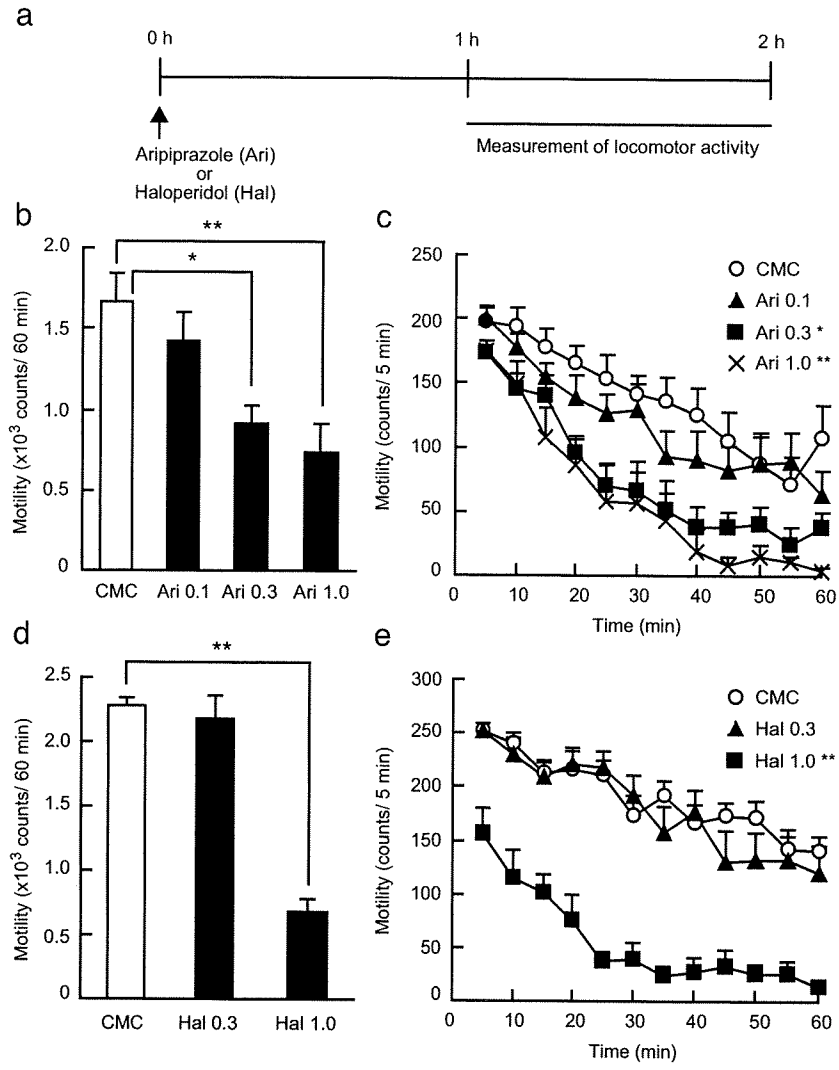

Fig. 1 Effects of single administration of aripiprazole and haloperidol on locomotor activity. **a** Experimental schedule for the measurement of locomotor activity. Mice were administered aripiprazole (*Ari*, 0.1–1.0 mg/kg, p.o.), haloperidol (*Hal*, 0.3–1.0 mg/kg, p.o.) or vehicle (0.1% *CMC*) 1 h before the measurement of locomotor activity. **b** and **c** Effect of single administration of aripiprazole on locomotor activity. **d** and **e** Effect of single administration of haloperidol on locomotor activity. **b** and **d** Total locomotor activity for 1 h. **c** and **e**: Time course of changes in locomotor activity. Values indicate the mean±SE (n=11–12). Analysis of variance: group, $F(3,43)=7.323$, $p<0.01$ for (**c**); time, $F(11,473)=58.971$, $p<0.01$ for (**c**); group × time, $F(33,473)=1.168$, $p=0.24$ for (**c**); group, $F(2,27)=46.806$, $p<0.01$ for (**e**); time, $F(11,297)=24.709$, $p<0.01$ for (**e**); group × time, $F(22,297)=1.370$, $p=0.13$ for (**e**). $^{*}p<0.05$ and $^{**}p<0.01$ compared with CMC group

To examine the role of dopamine D_1, D_2, and serotonin 5-HT_{1A} receptors in ameliorating the effect of aripiprazole on PCP-induced cognitive impairment, SCH23390 (0.03mg/kg), a dopamine D_1 receptor antagonist, raclopride (0.3mg/kg), a dopamine D_2 receptor antagonist, or WAY100635 (0.6mg/kg), a serotonin 5-HT_{1A} receptor antagonist, was administered intraperitoneally (i.p.) 30min after treatment with aripiprazole (0.1mg/kg, p.o.) for 7days because brain concentration of aripiprazole is the maximum at 2–3h after the oral administration, and declined $t_{1/2}$ of 1.8–2.0h in rats (Shimokawa et al. 2005). One day after the last treatment with aripiprazole and dopamine or serotonin receptor antagonists, the novel object recognition test was performed. The number of animals included in each drug treatment was as follows: saline + CMC + DW (n = 11), PCP + CMC + DW (n = 11), PCP + CMC + SCH23390 (n = 11), PCP + aripiprazole + DW (n = 11), PCP + aripiprazole + SCH23390 (n = 11) for Fig. 5b,d; saline + CMC + DW (n = 9), PCP + CMC + DW (n = 9), PCP + CMC + raclopride (n = 10), PCP + aripiprazole + DW (n = 9), PCP + aripiprazole + raclopride (n = 10) for Fig. 5c,e; saline + CMC + DW (n = 10), PCP + CMC + DW (n = 10), PCP + CMC + WAY100635 (n = 9), PCP + aripiprazole + DW (n = 10), PCP + aripiprazole + WAY100635 (n = 10) for Fig. 6.

Statistical analysis

All data were expressed as the mean±SEM. Statistical significance was determined using analysis of variance (ANOVA) with repeated measures (Figs. 1c,e, and 2c,e) or one-way (Figs. 1b,d, 2b,d, and 3–6), followed by the Bonferroni/Dunn test when F ratios were significant ($p<0.05$).

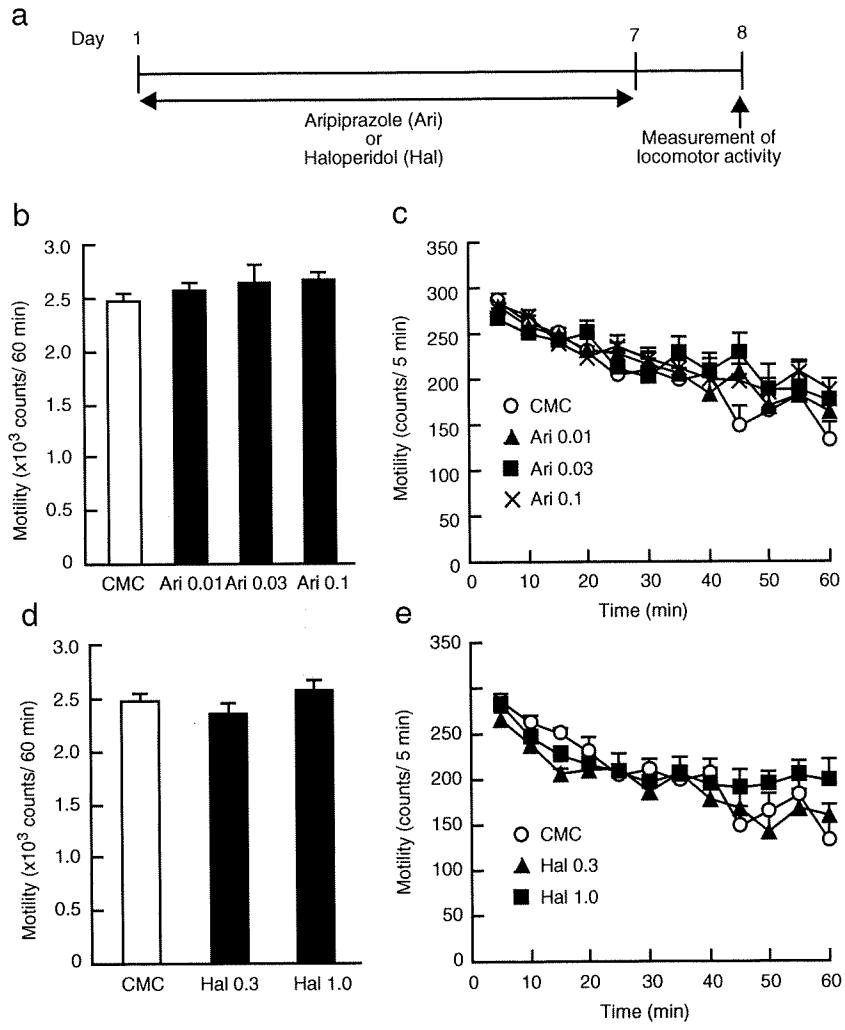

Fig. 2 Effects of repeated administration of aripiprazole and haloperidol on locomotor activity. **a** Experimental schedule for the measurement of locomotor activity. Mice were administered aripiprazole (*Ari*, 0.01–0.1 mg/kg, p.o.), haloperidol (*Hal*, 0.3–1.0 mg/kg, p.o.) or vehicle (0.1% *CMC*) for 7 days. Locomotor activity was measured 24 h after the last treatment. **b** and **c** Effect of repeated administration of aripiprazole on locomotor activity. **d** and **e** Effect of repeated administration of haloperidol on locomotor activity. **b** and **d** Total locomotor activity for 1 h. **c** and **e** Time course of changes in locomotor activity. Values indicate the mean±SE (n=10). Analysis of variance: group, $F(3,35)=0.743$, $p=0.53$ for (**c**); time, $F(11,385)=24.376$, $p<0.01$ for (**c**); group × time, $F(33,375)=1.099$, $p=0.33$ for (**c**); group, $F(2,27)=1.290$, $p=0.29$ for (**e**); time, $F(11,297)=18.444$, $p<0.01$ for (**e**); group × time, $F(22,297)=1.318$, $p=0.16$ for (**e**)

Results

Effects of administration of aripiprazole and haloperidol on locomotor activity

To explore the dose of aripiprazole and haloperidol which did not cause sedation in mice, we measured locomotor activity after oral administration of aripiprazole. Figure 1b and c shows the effect of a single administration of aripiprazole on locomotor activity in mice. Treatment with aripiprazole decreased total locomotor activity in a dose-dependent manner [$F(3,43)=7.323$, $p<0.01$, Fig. 1b]. The time course of changes in locomotor activity revealed that aripiprazole at doses of 0.3 and 1.0 mg/kg caused marked locomotor suppression 1 h after treatment [effect of group: $F(3,43)=7.323$, $p<0.01$; effect of time: $F(11,473)=58.971$, $p<0.01$; effect of interaction between group and time: $F(33,473)=1.168$, $p=0.24$ by two-way ANOVA with repeated measures, Fig. 1c]. Single treatment with haloperidol also decreased total locomotor activity in a dose-dependent manner [$F(2,27)=46.806$, $p<0.01$, Fig. 1d]. The time course of changes in locomotor activity revealed that haloperidol at the dose of 1.0 mg/kg caused marked locomotor suppression 1 h after treatment [effect of group: $F(2,27)=46.806$, $p<0.01$; effect of time: $F(11,297)=24.709$, $p<0.01$; effect of interaction between group and time: group × time, $F(22,297)=1.370$, $p=0.13$ by two-way ANOVA with repeated measures, Fig. 1e].

Effects of repeated administration of aripiprazole and haloperidol on locomotor activity were also examined. Mice were administered 0.1% CMC, aripiprazole (0.01–0.1 mg/kg, p.o.) or haloperidol (0.3–1.0 mg/kg, p.o.) was administered for 7 days. Locomotor activity was recorded 24 h after the last treatment. In contrast to the single treatment, repeated treatment with aripiprazole (0.01–0.1 mg/kg) and haloperidol (0.3–1.0 mg/kg) had no effect on the locomotor activity (Fig. 2).

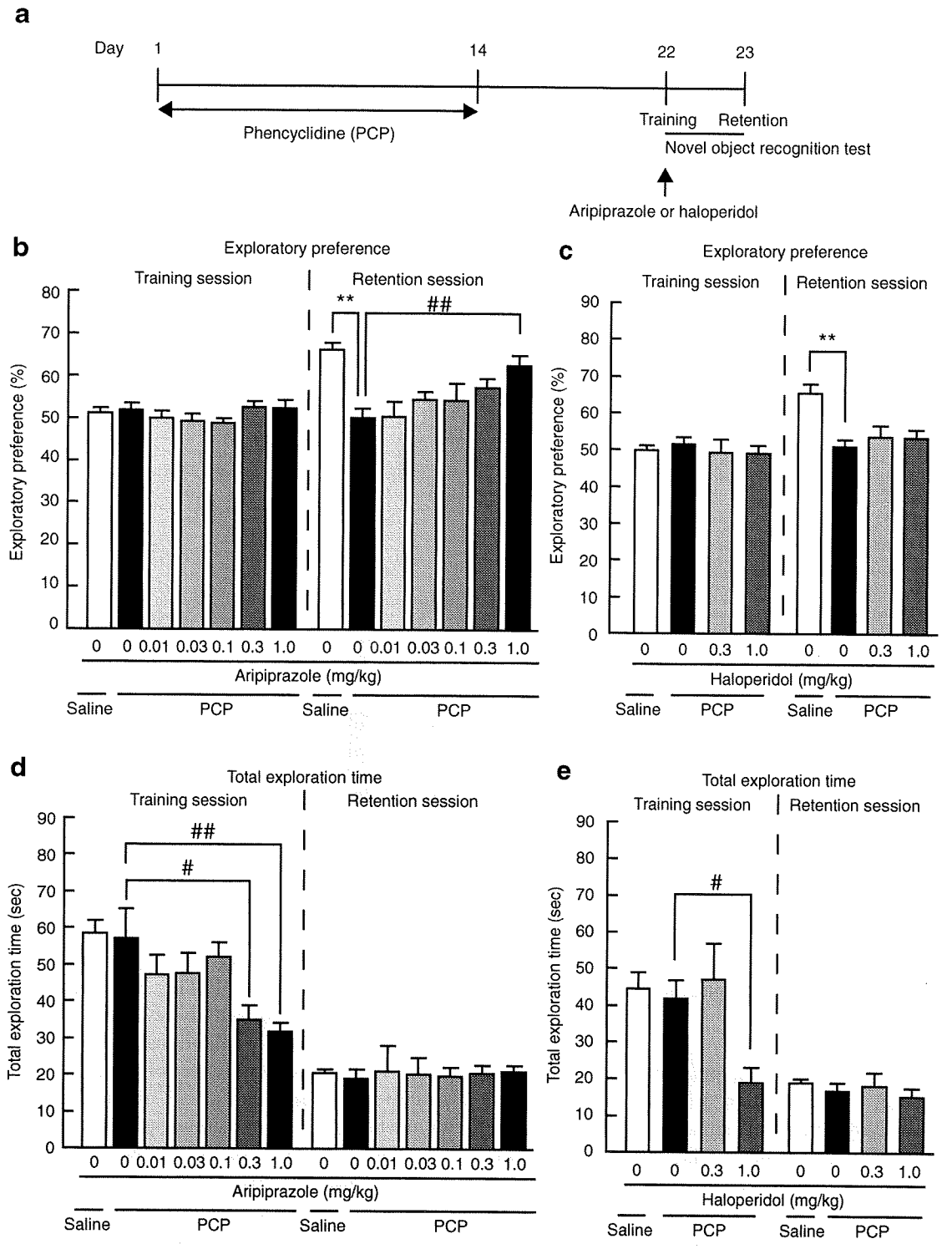

Fig. 3 Effects of single administrations of aripiprazole and haloperidol on PCP-induced cognitive impairment in novel object recognition. **a** Experimental schedule for the novel object recognition test. Eight days after withdrawal from repeated PCP (10 mg/kg, s.c., for 14 days) treatment, mice were subjected to the novel-object recognition test. Aripiprazole (0.01–1.0 mg/kg, p.o.), haloperidol (0.3–1.0 mg/kg, p.o.), or vehicle (0.1% CMC) was administered 1 h before the training session. **b** and **d** Effect of aripiprazole on PCP-induced cognitive impairment. **c** and **e** Effect of haloperidol on PCP-induced cognitive impairment. **b** and **c** Exploratory preference. **d** and **e** Total exploration time. Values indicate the mean±SE (n=8–16). Analysis of variance: $F(6,77)=0.911$, $p=0.49$ for (**b**) training; $F(6,77)=7.304$, $p<0.01$ for (**b**) retention; $F(3,39)=0.303$, $p=0.82$ for (**c**) training; $F(3,39)=8.69$, $p<0.01$ for (**c**) retention; $F(6,77)=5.009$, $p<0.01$ for (**d**) training; $F(6,77)=0.057$, $p=0.99$ for (**d**) retention; $F(3,39)=4.665$, $p<0.01$ for (**e**) training; $F(3,39)=0.600$, $p=0.62$ for (**e**) retention. $^{**}p<0.01$ compared with saline + vehicle group. $\#p<0.05$ and $\#\#p<0.01$ compared with PCP + vehicle group